GEO 610: Master's Thesis

Using multitemporal Sentinel-1 C-band backscatter to monitor phenology and classify deciduous and coniferous forests in northern Switzerland

Remote Sensing Laboratories
Department of Geography
University of Zurich

31 July 2017

Author:	Marius Rüetschi
Matriculation-Nr:	11-715-695
E-Mail:	marius.rueetschi@gmx.ch

Supervisor:	Dr. David Small
Faculty representative:	Prof. Dr. Michael E. Schaepman

Abstract

Efficient methods to monitor forested areas help us to better understand their processes. To date, only few studies have assessed the usability of multitemporal synthetic aperture radar (SAR) datasets in this context. Here we present an analysis of an unprecedented set of C-band observations of mixed temperate forests. We demonstrate the potential of using multitemporal C-band VV/VH polarisation data for monitoring phenology and classifying forests in northern Switzerland. The SAR images were radiometrically terrain corrected and a temporal compositing approach was applied. Several descriptors were calculated to extract the temporal signatures of European beech (*Fagus sylvatica*), oak (*Quercus robur, Quercus petraea*) and Norway spruce (*Picea abies*) in C-band data. Using their distinct seasonal signatures, the timing of leaf emergence and leaf fall of the deciduous species were estimated and compared to available ground observations. Furthermore, forest type and species classifications using random forest classifiers were implemented. The deciduous species backscatter was about 1 dB higher than spruce throughout the year in both polarisations. The forest types showed opposing seasonal backscatter behaviours. At VH, deciduous species showed higher backscatter in winter than in summer, whereas spruce showed higher backscatter in summer than in winter. In VV, this pattern was similar for spruce, while no distinct seasonal behaviour was apparent for the deciduous species. The time differences between the estimations and the ground observations of the phenological events were approximately within the error margin (± 12 days) of the used temporal resolution. The classification performances were promising, with higher accuracies achieved for the forest types (OA of 86% and $\kappa = 0.73$) than for individual species (OA of 72% and $\kappa = 0.58$). These results show that multitemporal C-band absolute backscatter data has significant potential to supplement optical remote sensing data for ecological studies and mapping of mixed temperate forests.

Zusammenfassung

Effiziente Waldbeobachtungsmethoden helfen uns, ein besseres Verständnis für die Prozesse in bewaldeten Flächen zu erlangen. Nur wenige Studien haben sich bisher damit auseinandergesetzt, ob dafür auch multitemporale *synthetic aperture radar* (SAR)-Daten in Frage kommen. Die vorliegende Studie hat sich dieser Frage angenommen, indem Zeitreihen von C-Band-Aufnahmen gemässigter Mischwälder einer noch nie dagewesenen Länge analyisert wurden. Wir zeigen, wie C-Band-Daten in VV/VH-Polarisation genutzt werden können, um die Phänologie zu beobachten und um die Wälder in der Nordschweiz zu klassifizieren. Die SAR-Bilder wurden radiometrisch Terrain-basiert normalisiert. Zudem kam eine Methode zur Anwendung, welche Bilder einer gewissen Zeitspanne miteinander kombiniert. Mittels deskriptiver Statistik wurden zeitliche Rückstreusignaturen der Arten Rotbuche (*Fagus sylvatica*), Eichen (*Quercus robur, Quercus petraea*) und Gemeine Fichte (*Picea abies*) aus den C-Band-Daten gewonnen. Die saisonal ausgeprägten Rückstreusignaturen der laubwerfenden Arten ermöglichten Schätzungen der Zeitpunkte der Blattentfaltung und des Blattfalls, welche dann mit bereits vorhandenen Bodenbeobachtungen verglichen wurden. Zudem wurden mithilfe des *Random Forest*-Klassifikationsverfahrens eine Waldtyp- und eine Artenklassifikation durchgeführt. Die jährliche Rückstreuung der laubwerfenden Arten war im Mittel etwa 1 dB höher als diejenige der Fichten in beiden Polarisationen. Ausserdem zeigten die beiden Waldtypen saisonal unterschiedliches Verhalten in der Rückstreuung. In VH war die Rückstreuung der laubwerfenden Arten höher im Winter und tiefer im Sommer, wohingegen Fichten höhere Rückstreuung im Sommer und tiefere im Winter zeigten. In VV war dieses Muster ähnlich für Fichten. Für die laubwerfenden Arten wurde jedoch kein saisonal ausgeprägtes Rückstreuverhalten registriert. Die zeitlichen Differenzen zwischen den geschätzten Phänologieereignissen und den Bodenbeobachtungen lagen im Bereich von ungefähr ± 12 Tagen. Dies entsprach der Genauigkeit, die durch die zeitliche Auflösung definiert war. Die Klassifikationsresultate waren vielversprechend. In der Waldtypenklassifikation (OA von 86% und $\kappa = 0.73$) wurde eine höhere Genauigkeit erreicht als in der Artenklassifikation (OA von 72% und $\kappa = 0.58$). Diese Resultate zeigen auf, dass im Gebrauch von multitemporalen C-Band-Daten erhebliches Potenzial steckt: Die Daten optischer Fernerkundung könnten ergänzt oder sogar ersetzt werden, was sowohl für ökologische Studien als auch für die Kartierung von gemässigten Mischwäldern von Interesse sein kann.

Table of Contents

List of Figures

List of Tables

List of Abbreviations

BD ..... Break date
BE ..... Canton of Bern (Switzerland)
CLC ..... CORINE land cover
CORINE ..... Coordination of Information on the Environment
DBH ..... Diameter at breast height
DHM ..... Digital height model
DLR ..... German aerospace centre
ENVISAT ..... Environmental satellite
ERS ..... European remote sensing satellites
ESA ..... European space agency
GDAL ..... Geospatial data abstraction library
GRDH ..... Ground range detected high resolution
GTC ..... Geocoded-terrain-corrected
HH ..... Horizontal transmitted, horizontal received (polarisation)
IW ..... Interferometric wide swath (Sentinel-1)
LAI ..... Leaf area index
LE ..... Leaf emergence
LF ..... Leaf fall
LRW ..... Local resolution weighting
MODIS ..... Moderate Resolution Imaging Spectroradiometer
NDVI ..... Normalised Difference Vegetation Index
OA ..... Overall accuracy
PA ..... Producer's accuracy
PAI ..... Plant area index
RF ..... Random forest
RTC ..... Radiometrically terrain corrected

SAR ..... Synthetic aperture radar
S-1 ..... Sentinel-1
SRTM ..... Shuttle Radar Topography Mission
UA ..... User's accuracy
VH ..... Vertical transmitted, horizontal received (polarisation)
VV ..... Vertical transmitted, vertical received (polarisation)
ZH ..... Canton of Zurich (Switzerland)

1 | Introduction

Climate change is affecting almost certainly most of the world's ecosystems (IPCC, 2014). It is leading to changes in phenology (Garonna et al., 2016) as well as shifts in species composition (Hansen et al., 2001). At the same time, these ecosystems provide valuable goods and services to human society (Costanza et al., 1997). Hence, the quantification of ecosystem changes is of great interest. It is therefore essential to find methods that accurately characterise the states of these systems. Spaceborne remote sensing is an efficient method for this purpose (Kellndorfer et al., 1998). It allows periodic acquisitions and is able to reach remote areas at low cost (Lu, 2006).

The European space agency (ESA) launched a series of new satellites in the framework of the earth observation programme Copernicus (Berger et al., 2012). Sentinel-1A was the first satellite launched, in April 2014. It carries a C-band synthetic aperture radar (SAR) sensor. Two years later, Sentinel-1B, was launched and completed the Sentinel-1 (S-1) constellation. Since autumn 2014, S-1 C-band SAR data has been publicly available in vertical-vertical (VV) and vertical-horizontal (VH) polarisation, acquired over the earth's landmasses. S-1 provides data continuity building on the previous C-band ERS and ENVISAT missions. But compared with them, S-1 offers improved spatial resolution, higher temporal resolution and enhanced radiometric calibration stability (Torres et al., 2012). All these properties are valuable improvements that facilitate the compilation of time series at a variety of spatial and temporal scales.

Analyses of time series allow regular monitoring of ecosystems but also have potential to reveal *temporal* signatures of land cover (Sharma et al., 2005; Gamba et al., 2008). These analyses can detect changes and help to gain insight into processes at work in numerous land ecosystems. These changes include intra-annual ones such as soil moisture alterations (Moran et al., 2000), but also inter-annual long-term trends such as shifts in biodiversity (Hansen et al., 2001).

In the context of climate change, forest ecosystems play a prominent role. They are

strongly influenced by climate change, observed in changes in phenology (Kramer, 1995) as well as shifts in forest species composition (Thom et al., 2016). They also contain about 90% of the world's vegetation carbon stock (IPCC, 2000). So their functional state and their distribution profoundly influence the global carbon cycle. Hence, characterising the states of forest ecosystems and their temporal evolution are of great interest.

Time series of remotely sensed data have potential to serve this purpose of characterising forest ecosystems. Time series of SAR data are promising, as SAR is acquired independent of weather and daylight (Kellndorfer et al., 1998) and sensitive to vegetation structure (Dobson et al., 1992). However, only few studies have analysed extended C-band time series of forested areas.

This thesis presents results of time series analyses of Sentinel-1 C-band VV and VH backscatter. The main focus was laid on the potential of multitemporal C-band data to characterise mixed temperate forests in northern Switzerland. The aims were

1. to analyse the different temporal backscatter behaviours of three different tree species,
2. to predict leaf emergence in spring and leaf fall in autumn using the distinct seasonal VH backscatter pattern of deciduous species and
3. to classify mixed temperate forests using the observed differences between forest types and species.

Our results show that multitemporal Sentinel-1 data can contribute to map and monitor forests.

The main findings are presented in chapter 2 and will be submitted to the peer-reviewed journal 'Remote Sensing'. The supplementary materials in chapter 3 present additional results concerning the temporal behaviour of backscatter of mixed temperate forests. Chapter 3 also contains results of leaf emergence characterisation using hemispherical images and it includes plots of temporal backscatter behaviour of several land cover types in the Alpine region. Chapter 4 briefly summarises new insights and illustrates future potential and upcoming challenges.

2 | Using multitemporal Sentinel-1 C-band backscatter to monitor phenology and classify deciduous and coniferous forests in northern Switzerland

This chapter is based on:

Rüetschi, M., Schaepman, M. E. & Small, D. (in preparation).

Using multitemporal Sentinel-1 C-band backscatter to monitor phenology and classify deciduous and coniferous forests in northern Switzerland.

To be submitted to:

Remote Sensing

Contribution:	
Design	70%
Materials & Methods	80%
Results & Conclusions	90%

Abstract

Efficient methods to monitor forested areas help us to better understand their processes. To date, only few studies have assessed the usability of multitemporal synthetic aperture radar (SAR) datasets in this context. Here we present an analysis of an unprecedented set of C-band observations of mixed temperate forests. We demonstrate the potential of using multitemporal C-band VV/VH polarisation data for monitoring phenology and classifying forests in northern Switzerland. The SAR images were radiometrically terrain corrected and a temporal compositing approach was applied. Several descriptors were calculated to extract the temporal signatures of European beech (*Fagus sylvatica*), oak (*Quercus robur, Quercus petraea*) and Norway spruce (*Picea abies*) in C-band data. Using their distinct seasonal signatures, the timing of leaf emergence and leaf fall of the deciduous species were estimated and compared to available ground observations. Furthermore, forest type and species classifications using random forest classifiers were implemented. The deciduous species backscatter was about 1 dB higher than spruce throughout the year in both polarisations. The forest types showed opposing seasonal backscatter behaviours. At VH, deciduous species showed higher backscatter in winter than in summer, whereas spruce showed higher backscatter in summer than in winter. In VV, this pattern was similar for spruce, while no distinct seasonal behaviour was apparent for the deciduous species. The time differences between the estimations and the ground observations of the phenological events were approximately within the error margin (± 12 days) of the used temporal resolution. The classification performances were promising, with higher accuracies achieved for the forest types (OA of 86% and $\kappa = 0.73$) than for individual species (OA of 72% and $\kappa = 0.58$). These results show that multitemporal C-band absolute backscatter data has significant potential to supplement optical remote sensing data for ecological studies and mapping of mixed temperate forests.

Keywords Sentinel-1, SAR, C-band VV/VH backscatter, forest mapping, temporal signature, classification, phenology, leaf emergence, leaf fall, mixed temperate forest

2.1 Introduction

Forests provide valuable ecosystem goods and services for human well-being (Stenger et al., 2009). Therefore, it is of great interest to gather information about the state of the forest ecosystems. Because forest inventories are costly, it is essential to develop cost-effective mapping methods to allow management of forests (Gudex-Cross et al., 2017). In times of climate change, periodic assessments are in demand, as changes in phenology (Kramer, 1995; Garonna et al., 2016) as well as shifts in species composition (Hansen et al., 2001; Thom et al., 2016) become apparent. It is important to discover efficient ways to continually monitor forested areas and subsequently gain knowledge about processes and changes.

Remote sensing offers valuable tools to implement mapping and monitoring approaches (Kasischke et al., 1997). Until now, mainly optical sensors have been used to monitor forests on a global scale, ranging from intra-annual studies (Cristiano et al., 2014; Hobi et al., 2017) to others examining several years (de Jong et al., 2011; Garonna et al., 2016). Using optical sensors however, two main disadvantages are apparent. First, optical sensors are not sensitive to vegetation structure. Second, temporally consistent data acquisition is challenging, as the optical sensor's views are often impaired by cloud cover. To overcome these disadvantages, it is important to consider synthetic aperture radar (SAR). SAR is sensitive to vegetation structure (Dobson et al., 1992) and is acquired independent of daylight and weather, so it can more easily produce temporally consistent data (Kellndorfer et al., 1998).

Until now, SAR data has predominantly been used to analyse and monitor tropical (Luckman et al., 1997; Englhart et al., 2011; Reiche et al., 2013) and boreal forests (Maghsoudi et al., 2013; Antropov et al., 2014; Thiel & Schmullius, 2016). Because of frequent cloud coverage, SAR has to be considered in the tropics. In the northern boreal forests, however, SAR is also relevant, as long periods with sparse or no daylight pose a further barrier to using optical remote sensing data. It is useful to assess the potential of SAR data for mixed temperate forests, as only a few studies assessing this potential have been conducted until now (Proisy et al., 2000; Dostálová et al., 2016). Given that significant structural changes due to phenology happen within a short time period in spring and autumn, reliable observations are critical.

The two recently launched Sentinel-1 (S-1) satellites, carrying C-band SAR sensors, offer new possibilities in the compilation of time series. Generally, they acquire backscatter

in vertical-vertical (VV) and vertical-horizontal (VH) polarisation mode over landmasses (ESA, 2017). S-1 data has already been successfully applied to several land applications. It has been used to monitor crop growth of several cultures in Angola (Navarro et al., 2016) and of rice in Myanmar (Torbick et al., 2017). Balzter et al. (2015) and Abdikan et al. (2016) showed that using S-1 data leads to satisfying classification of land cover classes. Other studies exhibited the potential of S-1 data for burnt area mapping in forests (Verhegghen et al., 2016), monitoring wetlands (Muro et al., 2016) or snow wetness estimation in the Alps (Jäger, 2016; Rondeau-Genesse et al., 2016). S-1 offers superiour spatial and temporal coverage and much improved radiometric calibration stability in comparison to former spaceborne C-band sensors (Torres et al., 2012).

Previous work has shown that SAR forest backscatter is very complex, being dependent on several sensor and object properties. Generally, sensors with high frequencies such as X- or C-band are less able to penetrate the crown than are lower frequencies such as S- or L-band (Solimini, 2016). Thus, the dominance of the crown return is stronger at high frequencies. The polarisation used by the SAR sensor also impacts the backscatter. Cross-polarised backscatter from forested areas leads to higher correlation with biomass than co-polarised backscatter (Leckie & Ranson, 1998). Object properties impacting forest backscatter can be divided into two groups. The first group consists of properties that influence the dielectric constant of the trees, such as the moisture content of branches and leaves (Proisy et al., 2000), external moisture conditions (Sharma et al., 2005), and the temperature of the wood (Way et al., 1990; Olesk et al., 2015). The second group consists of structural properties such as the size and orientation of branches and leaves (Imhoff, 1995), the spatial pattern of trees (Westman & Paris, 1987), and whether or not foliage is present (Chuah & Tan, 1992; Ahern et al., 1993). The last is especially interesting, as it could allow the monitoring of phenology at a land surface scale.

Until now, most studies with the aim of mixed temperate forest characterisation have focused on extracting additional information by using multiple polarisations (Touzi et al., 2004; Cable et al., 2014; Varghese & Joshi, 2015). Collecting multiple SAR acquisitions into longer time series has the potential to reveal *temporal* signatures (Sharma et al., 2005; Gamba et al., 2008). However, only few studies have analysed longer C-band time series of forested areas. Ahern et al. (1993) and Proisy et al. (2000) found phenology effects on C-band SAR backscatter for coniferous and deciduous forest types using horizontal-horizontal (HH) and VV polarisation mode, respectively. A recent study us-

ing S-1 data showed the impact of phenology of deciduous forests to be much higher in cross-polarised than in co-polarised data (Dostálová et al., 2016).

In this paper, we present an analysis of Sentinel-1 SAR absolute backscatter time series of an unprecedented set of VV and VH polarisation observations over mixed temperate forests in northern Switzerland. One coniferous and two broad-leaved, deciduous species were investigated. We show how to build the C-band time series and to subsequently extract descriptors for the different forests investigated. A detailed analysis of these descriptors is provided, focusing on differences between tree species and between the investigated years. Finally, we show how our findings help to classify mixed temperate forests and how they could help in future monitoring of the seasonal vegetation cycles of forests.

2.2 Materials and Methods

2.2.1 Study areas

The areas studied were the whole of the Canton of Zurich (ZH), and three forest stands in the Canton of Bern (BE) in Switzerland. For the main analysis, two areas in the north of ZH and the three stands in BE were used. This led to five different main study areas with forest stands of variable extents across northern Switzerland being evaluated (Table 2.1 and Figure 2.1). All these study areas consist of temperate mixed forest stands with different predominant species. The forest stands considered for more detailed investigations were relatively homogenous, having a relative high proportion of a single species. In addition to that, the extent of the forest stands had to be large enough to allow an erosion of edge pixels (see section 2.2.3.2 for details) to limit border effects. The three predominant species examined were European beech (*Fagus sylvatica*), oak (*Quercus robur, Quercus petraea*) and Norway spruce (*Picea abies*). The elevations of the different study areas did not differ significantly, ranging from 390 to 670 m a.s.l.

Table 2.1: The investigated study areas are distributed in northern Switzerland in the Cantons of Zurich (ZH) and Bern (BE). The listed values in the columns elevation, slope and diameter at breast height (DBH) are all mean values from the respective study area. The core extent describes the investigated extent after the applied erosion.

No.	Study area (Ca)	Species	Elevation (m a.s.l.)	Slope (°)	Core extent (ha)	DBH (cm)
1	Rafz (ZH)	Spruce	498	6.2	23.0	≥ 51
		Beech	474	12.8	13.5	41-50
		Oak	466	11.5	14.9	41-50
2	Teufen (ZH)	Spruce	596	12	46.7	41-50
		Beech	602	15.5	15.7	41-50
3	Galsberg (BE)	Beech	507	15.4	7.6	41-50
4	Feiberg (BE)	Beech	509	16.5	12.7	≥ 51
5	Büren a.d.A. (BE)	Oak	496	2.3	6.5	31-40

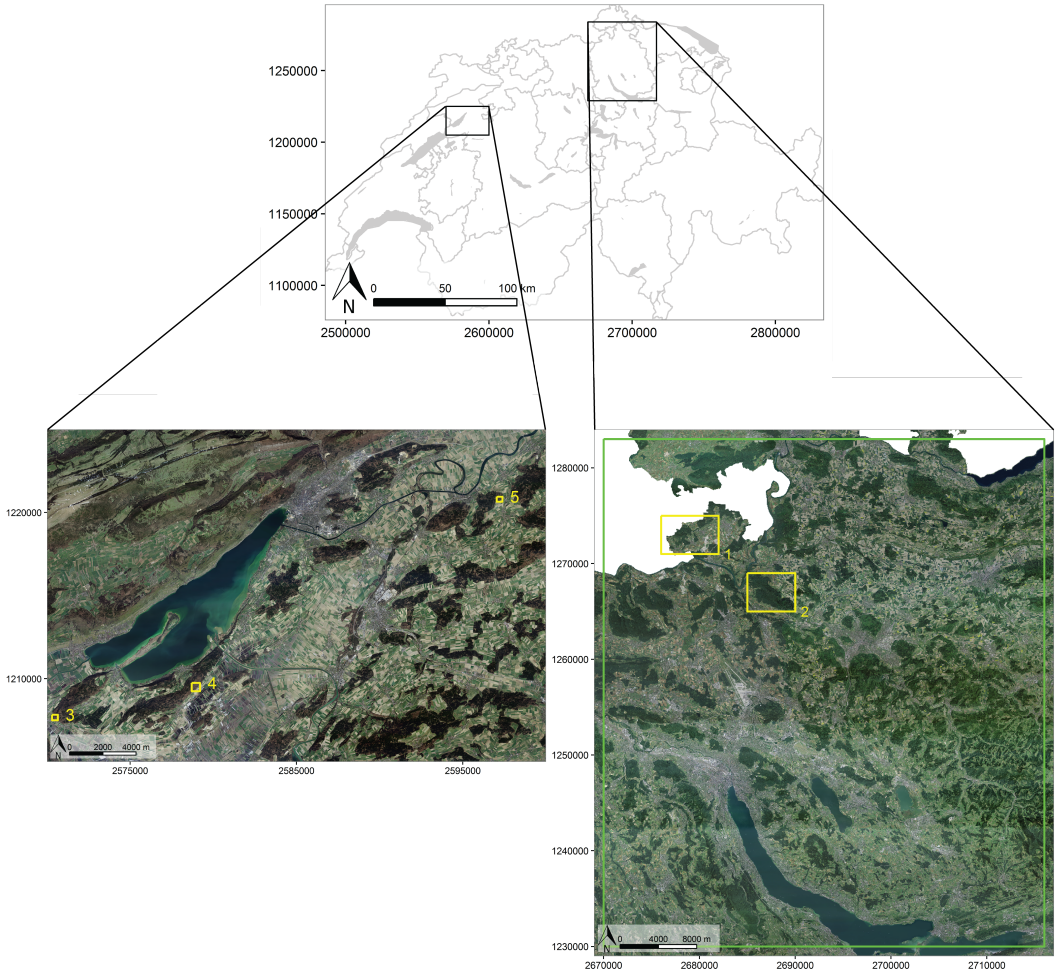

Figure 2.1: The five investigated main study areas are located within the yellow rectangles in the Cantons of Zurich (ZH) and Bern (BE) in northern Switzerland. For some analyses, the entire forested area within the Canton of Zurich, depicted in the green rectangle, was used. The background aerial images were provided by the Swiss Federal Office of Topography swisstopo (2010). Swiss map coordinates: CH1903+ / LV95.

2.2.2 Data

We used Sentinel-1 C-band Interferometric Wide (IW) swath mode Ground Range Detected High Resolution (GRDH) images covering the study areas. The chosen time span was between 01/01/15 and 24/05/17. Because both available polarisations were considered, 433 VV- and 433 VH-images were used as input to the investigation (Torres et al., 2012). The IW mode specifications are listed in Table 2.2.

Table 2.2: Specifications of Sentinel-1 IW mode (Torres et al., 2012)

Specification	**Value**
Swath width	250 km
GRDH sample distance	10 m
Nominal incident angle range	31°- 46°
Radiometric stability	0.5 dB (3σ)
Radiometric accuracy	1 dB (3σ)

To process the SAR data, a digital height model (DHM) was available with a spatial resolution of 2 m (Federal Office of Topography swisstopo, 2017). For the purpose of this study, this DHM was resampled to a spatial resolution of 10 m to match the resolution of the S-1 images.

In-depth information about the forests in the Canton of Zurich were provided by the aerial image forest stand map released by the Office of Landscape, Agriculture and Environment (2010) (*Amt für Landschaft und Natur*) of the Canton of Zurich. The vector dataset contains information about several characteristics of the forest stands such as relative tree species abundance, tree cover density and stand height. For this study, the dataset was converted into a raster layer with a spatial resolution of 10 m using the Geospatial Data Abstraction Library (GDAL) tool *rasterize* (GDAL, 2017).

Meteorological and phenological data of the study areas were also prepared. MeteoSwiss provided daily mean temperature and precipitation raster layers with a spatial resolution of 1.25', corresponding approximately to 2.3 km in northing and 1.6 km in easting (Federal Office of Meteorology and Climatology MeteoSwiss, 2017a). Both layers were produced by spatially interpolating data of the MeteoSwiss weather station network of Switzerland (Federal Office of Meteorology and Climatology MeteoSwiss, 2017b). Phenological observations were available, released by MeteoSwiss for selected weather stations (Federal Office of Meteorology and Climatology MeteoSwiss, 2017a). Observations

of the two stations *Rafz* and *Biel* were selected for this study based on their proximity ($<$ 25 km) to the investigated forest stands of the study areas 1, 3 and 4 (see Table 2.1). These observations contain annual information for the species beech and spruce. For beech, the timing of leaf emergence in spring, and leaf colouring and leaf fall in autumn is recorded by volunteers, for spruce, only needle shoot in spring.

2.2.3 Methods

In a first step, the SAR data was radiometrically calibrated and geocoded, and time series were built (Figure 2.2). Subsequently, masks were generated to analyse the backscatter behaviour of the different species and forest types. Then, temporal backscatter patterns in the different forests were assessed calculating several descriptors (Figure 2.4). In a last step, classifications were implemented by making use of the significant differences in the temporal backscatter signatures of the different species (Figure 2.6).

2.2.3.1 SAR data processing

The acquired Sentinel-1 IW VV and VH acquisitions were processed in two different ways, as illustrated in Figure 2.2. First, the acquisitions were radiometrically calibrated and terrain-geocoded with the available DHM, which resulted in geocoded-terrain-corrected (GTC) images for both polarisations (Meier et al., 1993). These GTC images had a pixel spacing of 10 m. Second, to reduce the strong influence of topography on the backscatter (Atwood et al., 2012), the VV and VH acquisitions were also radiometrically calibrated and terrain-geocoded according to the radiometric terrain flattening methodology described in (Small, 2011). This approach corrects not only the geometry of the scene but also its radiometry. The resulting radiometrically terrain corrected (RTC) images exhibit an easier interpretability, which is especially valuable in areas with complex terrain. The pixel spacing of these RTC images was also 10 m.

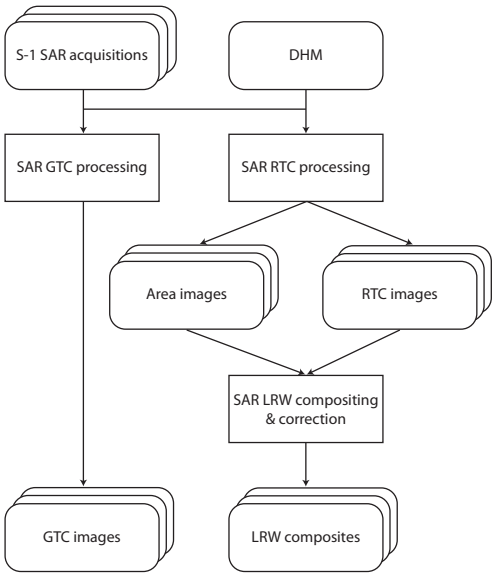

Figure 2.2: Processing scheme of the SAR data from S-1 GRDH images to GTC images and LRW composites. GRDH images of both polarisations were processed in this manner.

In a second stage, a multitemporal compositing approach was applied to the RTC images of both polarisations to enhance spatial resolution and reduce noise (Small, 2012). The local resolution weighting (LRW) approach combines RTC images of ascending and descending acquisitions within a specific timespan into composite backscatter images. A timespan of 24 days and a temporal sampling interval of 12 days were found to adequately observe seasonal backscatter behaviour while also ensuring full areal coverage, even when fewer images than typical were available due to calibration activities in southern Germany. The compositing led to reliable time series of SAR observations of the study areas. Only for a single 24 day period could no composite of the study areas in ZH be produced. Between 06/06/15 and 29/06/15 no acquisitions were available in northern ZH, due to a system calibration campaign of the German aerospace centre (DLR) in southern Germany (Schwerdt et al., 2017).

The evolution of the number of acquisitions available from 2015-2017 is shown in Figure 2.3. There are three reasons why the number of available acquisitions changed considerably over the investigated time period for both study areas. The low number of available acquisitions in summer 2015 (2 acquisitions) and 2016 (3 acquisitons) were caused by the DLR campaign. A gradual increase to a maximum of 18 acquisitions towards the end of the investigated time period was due to a (a) ramp-up of the production by

the European space agency (ESA) payload data ground segment and (b) the addition of Sentinel-1B acquisitions in September 2016 (Schubert et al., 2017).

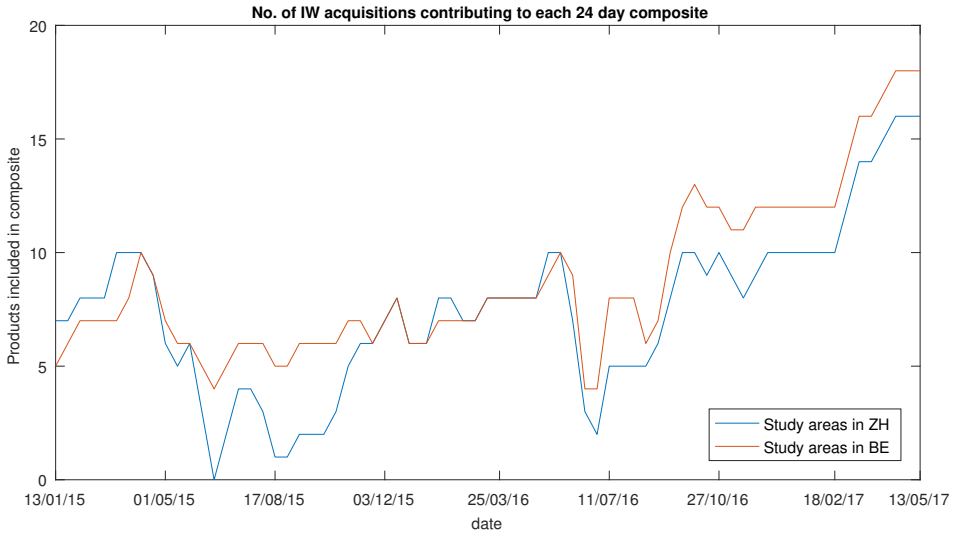

Figure 2.3: Evolution of the number of acquisitions available for the LRW compositing. The number of acquisitions available varied significantly for the study areas 1-2 in ZH and 3-5 in BE. Especially in summer 2015 but also in summer 2016, only few acquisitions were available. Generally, more acquisitions were available for the study areas in BE, and the number of available acquisitions increased towards the end of the investigated period in all study areas.

An absolute backscatter calibration issue was mitigated by applying corrections. Both Miranda (2015), and El Hajj et al. (2016) reported positive Sentinel-1A antenna gain biases between 19/03/15 and 25/11/15. Hence, all backscatter values within that timespan were corrected. After El Hajj et al. (2016), a correction of -0.9 dB was applied within that time period in 2015.

2.2.3.2 Species mask generation

To analyse the backscatter behaviour of GTC images and LRW composite time series, masks for the three different tree species and the two forest types were produced following a scheme shown in Figure 2.4. For the study areas in the Canton of Zurich, species and forest type masks were generated by segmenting the aerial image forest stand map. For the *species* masks, this was done by choosing all pixels with high species homogeneity for beech, oak and spruce. For the *forest type* masks, the considered forest stands consisted of either deciduous or coniferous species. Because there were not enough pixels of absolutely homogenous stands, pixels with species homogeneity greater than 80% were

chosen. The threshold of 80% was chosen, as a trade-off between the available number of pixels and ensuring a considerable dominance of the species within the forest stand. The masks for the study areas in BE were produced based on forest knowledge of local foresters (Schneider, 2016; Lüthi, 2017; Zwahlen, 2017). This spatial information about the forest stands was subsequently rasterised to produce the three masks.

All the masks were ”eroded” to minimise edge effects and ensure the presence of the desired species or forest type. This was done using an erode function with a square mask of 3x3 times the sample interval. Similar to the homogeneity threshold, the 3x3 size was chosen as a trade-off between maximising the available number of pixels and mitigating edge effects.

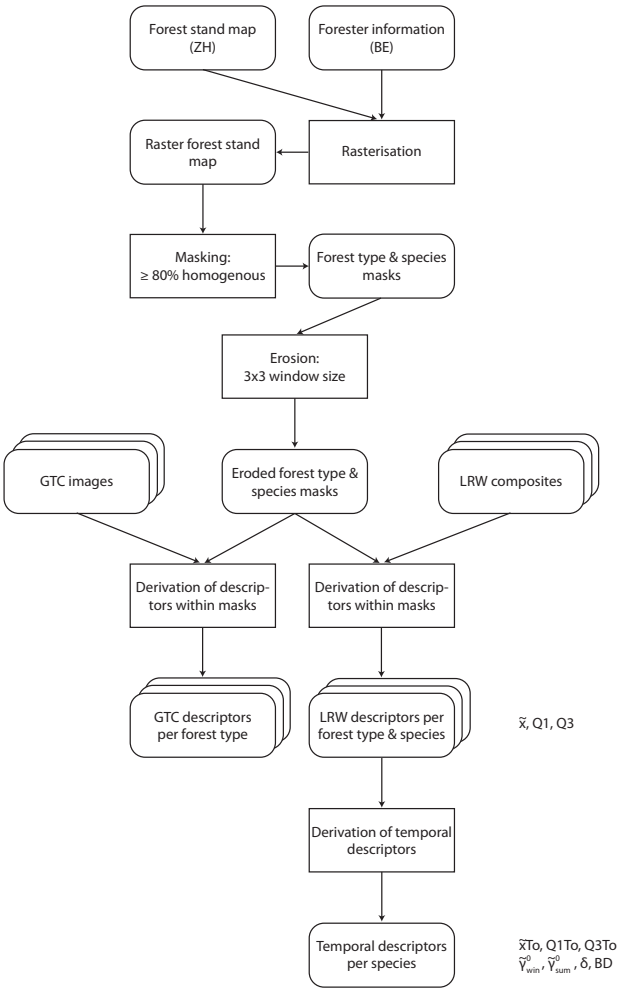

Figure 2.4: Processing chain for deriving the backscatter descriptors from the GTC images and LRW composite time series for different forest types and species. The descriptors shown on the right were derived from both polarisations.

2.2.3.3 Comparison of a winter and summer GTC image and LRW composite

In a first analysis, the backscatter of the forested area in the whole of ZH of two GTC images was compared. The chosen images were from 06/06/16 for summer/leaf-on and 16/03/17 for winter/leaf-off. The images were masked with the generated forest type masks and the median, 25 & 75% percentiles were calculated within the residual pixels ($\tilde{x}$, Q1, Q3). Subsequently, the medians were compared for the two dates and the two forest types. RGB-overlays and histograms were prepared to highlight differences in backscatter distribution between the two acquisition dates and between the two SAR processing methods. RGB-overlays and histograms were produced using the above-mentioned GTC images; others were generated using LRW composites of the timespans 24/05 - 16/06/16 and 02/03 - 25/03/17. In the RGB-overlays, the summer image was assigned to the red and blue channels, and the winter image was assigned to the green channel (Figure 2.5).

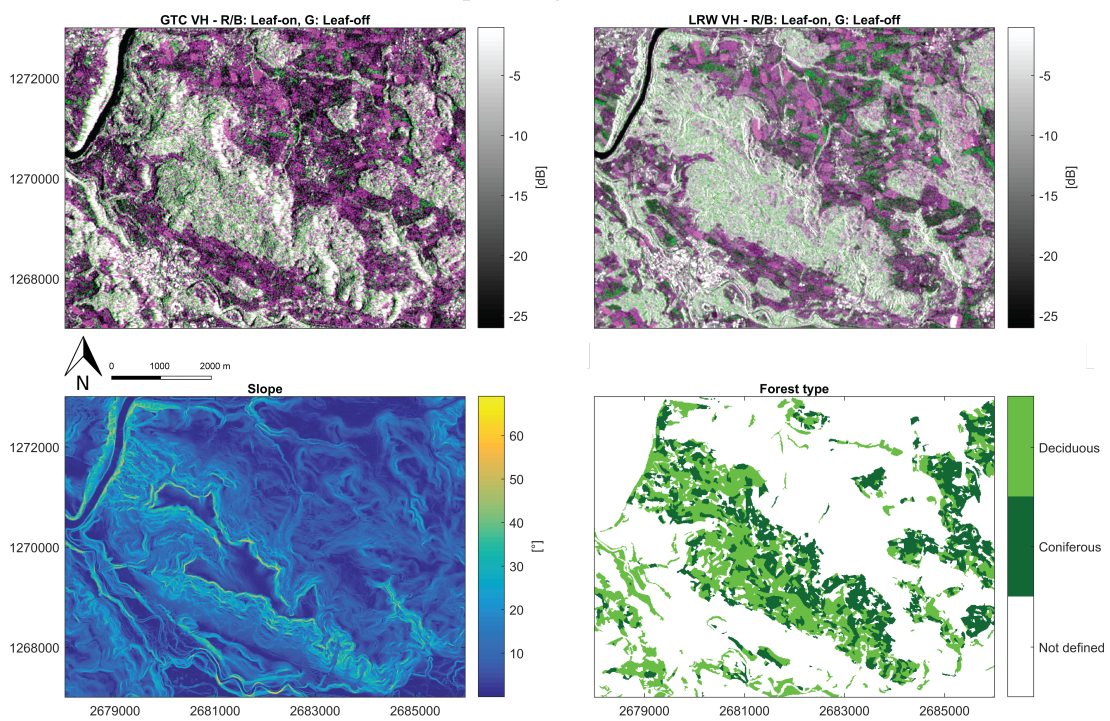

Figure 2.5: Top row: RGB-overlays of GTC images and LRW composites. The assigned bands are R/B = summer/leaf-on (GTC: 06/06/16, LRW: 24/05 - 16/06/16) , G = winter/leaf-off (GTC: 16/03/17, LRW: 02/03 - 25/03/17). In the lower row, maps of the main influencing factors on the backscatter are depicted. On the left, the slope map of the area is shown. On the right, the forest type map with the classes 'deciduous', 'coniferous' and 'not defined', consisting of all non-forested areas and areas with less than 50% homogenous species. Swiss map coordinates: CH1903+ / LV95.

The advantages of the RTC processing and the LRW compositing approach over the GTC-based processing are apparent. The colour pattern in the LRW RGB-overlay appears much smoother, leading to a better discrimination between the two forest types. In addition to that, the strong influence of topography on the GTC RGB-overlay is seen (e.g. steep slope right next to the river bed in the northwest). In areas with steep foreslopes (Figure 2.5, lower left), backscatter was higher. In the LRW RGB-overlay on the other hand, topographic effects were mitigated.

2.2.3.4 Time series analysis of LRW composites

In the main analysis, the temporal behaviour of the forest backscatter was investigated. The descriptors listed on the first row of Table 2.3 were calculated for every LRW composite within the eroded masks ($\tilde{x}$, Q1, Q3). Subsequently, these descriptors were plotted in the temporal domain and their seasonal behaviour was inspected visually. To analyse this behaviour further, the temporal descriptors listed in Table 2.3 on the second row were calculated for the previously established descriptor time series.

Table 2.3: Descriptors calculated within single composites and within the time series.

	Descriptors	**Symbols**
Within single composite	Median, 25 & 75% percentiles	$\tilde{x}$, Q1, Q3
Within time series	Median of $\tilde{x}$ and of Q1 & Q3	$\tilde{x}$To, Q1To, Q3To
	Median winter of $\tilde{x}$, median summer of $\tilde{x}$	$\tilde{\gamma}^0_{win}$, $\tilde{\gamma}^0_{sum}$
	δ (see Equation (2.1)), break dates	δ, BD1, BD2

The medians within the time series were derived from all the calculated medians and 25 & 75% percentiles of the masked composites ($\tilde{x}$To, Q1To, Q3To). The medians of winter ($\tilde{\gamma}^0_{win}$) and summer ($\tilde{\gamma}^0_{sum}$) were calculated, as visual inspection of the plots indicated a change in backscatter between the two seasons. The timespan for the two seasons was chosen conservatively to be 01/06 - 15/09 for summer and 01/12 - 15/03 for winter. This was done to ensure that no 'winter' composites with leaf-off conditions appeared in the 'summer' subset and vice versa. Their difference (δ) was calculated according to Equation (2.1).

$$\delta = \tilde{\gamma}^0_{winter} - \tilde{\gamma}^0_{summer} \tag{2.1}$$

The timing of the change in backscatter was also of interest. Natural breakpoints in the time series were calculated using the algorithm described in (Zeileis et al., 2002).

The function *breakpoints* allows detection of structural changes in time series of data (Zeileis et al., 2003) and has successfully been used in previous ecological studies (e.g. de Jong et al. (2013); Vanoni et al. (2016)). The time series were split into annual sets to facilitate detection of the break dates. The function assigns break dates where the OLS-based CUSUM test (Ploberger & Krämer, 1992) registers the two highest empirical fluctuation process values (Zeileis et al., 2003). The first break date within each time series was assumed to be the leaf emergence (BD1), while the second break date was assumed to be the leaf fall of the respective year (BD2). The missing value due to the absent LRW composite in summer 2015 for the study areas in ZH (1 & 2 in Table 2.1) was linearly interpolated (Zeileis et al., 2017) to facilitate use of the *breakpoints* algorithm.

The last step consisted of a comparison of the calculated descriptors for the different forests. General differences between deciduous and coniferous forests were compared as well as differences between the two deciduous species beech and oak. The phenological ground observations, when available, were juxtaposed with the *breakpoints*-based break dates.

2.2.3.5 Classification of species and forest type

We conducted two classifications of the forested areas in the Canton of Zurich using a random forest (RF) classifier (Breiman, 2001). In addition to a classification of the three species examined, another was performed on the forest types deciduous and coniferous. RF was chosen, as a study using multitemporal C-band SAR data showed that RF outperformed other classifiers (Waske & Braun, 2009). In addition to the actual classification, it also ranks the importance of the used predictors. We generated for both approaches a forest of 100 decision trees with a minimum terminal node size of 1 using the MATLAB class *TreeBagger* to perform the classification (Mathworks, 2017).

The classification processing chain is illustrated in Figure 2.6. First, twelve predictors were calculated per pixel within the LRW composite time series. The predictors used were (1-8) the respective median of the years 2015 and 2016 as well as the respective δ between winter (leaf-off) and summer (leaf-on) medians at both polarisations. The definition for the seasonal periods was again chosen conservatively, with 01/12 - 15/03 for winter and 01/05 - 15/09 for summer. Two break dates (9-12) for the two years were derived per pixel VH time series, using the *breakpoints* algorithm. These break dates completed the set of predictors.

Second, the training and validation datasets were prepared. This was done by gener-

ating forest masks, applying the erode function and subsequently random selecting pixels for the two datasets. The mask generation and erosion for both classifications approaches were performed uniformly as described in section 2.2.3.2. Then, different RF models were trained with a balanced number of randomly selected pixels for every model. Another balanced set of randomly selected pixels was then used to validate every model. This procedure was identically executed for the *forest type* and the *species* classification.

To ensure a representative estimation of the performances, the dependencies of the achieved mean accuracies on the number of RF models were evaluated. It showed that more than 40 models did not significantly change the mean accuracies ($\pm 0.25\%$). The number of RF models was set to 40 for both approaches. The performances of the two classifications and their utility were then evaluated by generating the mean confusion matrix and calculating mean overall accuracy, producer's accuracy, user's accuracy and Cohen's kappa of the 40 different RF models. The "predictor importance" measure was also assessed. For every predictor, that measure specifies the loss in prediction accuracy if the values of that predictor are distributed randomly across the pixels (Mathworks, 2017).

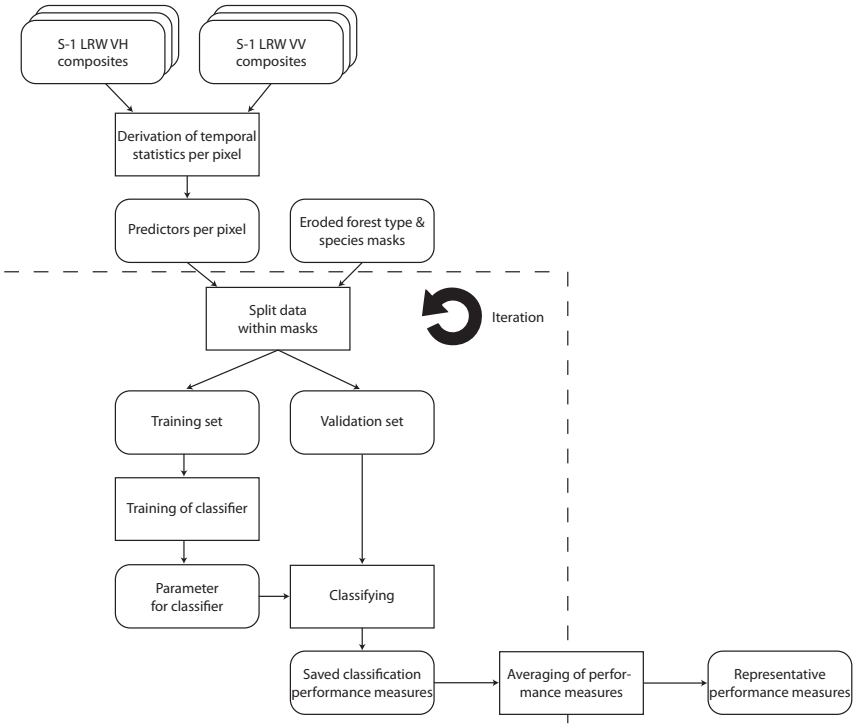

Figure 2.6: Classification scheme. This framework was used for both *forest type* and *species* classifications.

2.3 Results

2.3.1 Comparison of the seasonal GTC images and LRW composites

Table 2.4 shows the results of the calculation of the median, 25 & 75% percentiles backscatter within the forest type masks in the two GTC images for both polarisations. Generally deciduous species showed higher backscatter than coniferous stands. With the exception of VH polarisation in summer, the difference between the two forest types was quite substantial. A seasonal change in VH backscatter within both forest types was observed. Coniferous forests had stronger backscatter in summer (06/06/16) and lower in winter (16/03/17), whereas deciduous forests showed the opposite, with higher backscatter in winter and lower in summer.

Table 2.4: Median ($\tilde{x}$), 25 & 75% percentiles (Q1 & Q3) C-band VH/VV backscatter (GTC-images) for deciduous and coniferous forest stands of the whole of the Canton of Zurich. The investigated stands had a species homogeneity of at least 80%.

		Winter			**Summer**		
Forest type		**Q1**	$\tilde{x}$	**Q3**	**Q1**	$\tilde{x}$	**Q3**
Deciduous forest	VH	-14.0	**-12.3**	-10.6	15.0	**-13.3**	-11.6
	VV	-9.3	**-7.6**	-6.0	-9.1	**-7.2**	-5.4
Coniferous forest	VH	-15.7	**-14.2**	-12.6	-14.7	**-13.2**	-11.7
	VV	-10.3	**-8.8**	-7.3	-9.0	**-7.5**	-5.9

This seasonal change is also apparent in a VH GTC RGB-overlay (Figure 2.5, top left) and a LRW counterpart (Figure 2.5, top right) of the study area in Teufen. Areas in magenta showed higher backscatter in summer, whereas areas in green showed higher backscatter in winter. It can therefore be expected that areas in magenta consisted mainly of coniferous species, and areas in green mainly of deciduous species. Compared with the forest type map of the area (Figure 2.5, lower right), a striking correspondence is visible between the colour patterns of the RGB-overlays and the forest type classes.

The distribution of the backscatter values of the two forest types in the two SAR products is depicted in Figure 2.7. Two features are apparent. First, the seasonal shift from winter to summer to higher backscatter values for coniferous forests (first column), and the opposing seasonal shift to lower values for deciduous forests (second column) are seen. Second, the variance within the GTC images (first row) was substantially higher than in the LRW composites (second row). Especially for deciduous forests, the variance was much lower in the LRW composite. The seasonal shift is depicted per pixel in the difference between winter and summer VH backscatter of the two forest types (Figure 2.8). Values for deciduous and coniferous forests were mainly positive and negative, respectively. Again, the variance within the LRW composites was considerably lower. This is expected to allow a more reliable separability between the two forest types.

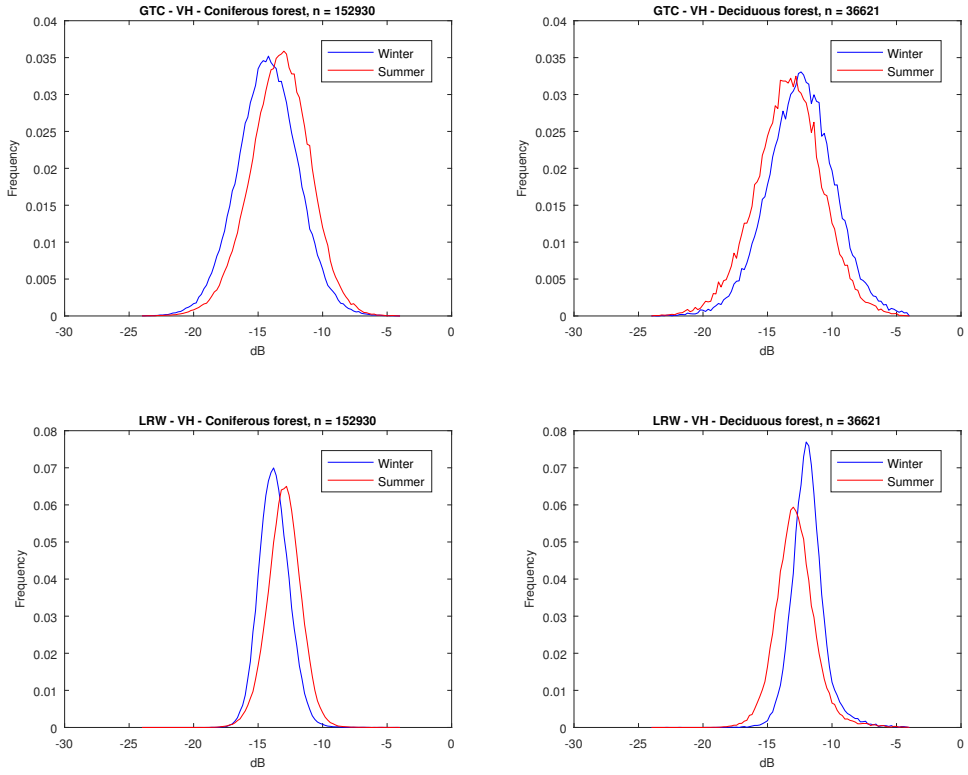

Figure 2.7: Histograms of the VH backscatter value distribution within the two forest types for the GTC images (first row) and the LRW composites (second row). The number of pixels (n) was considerably higher for coniferous forests.

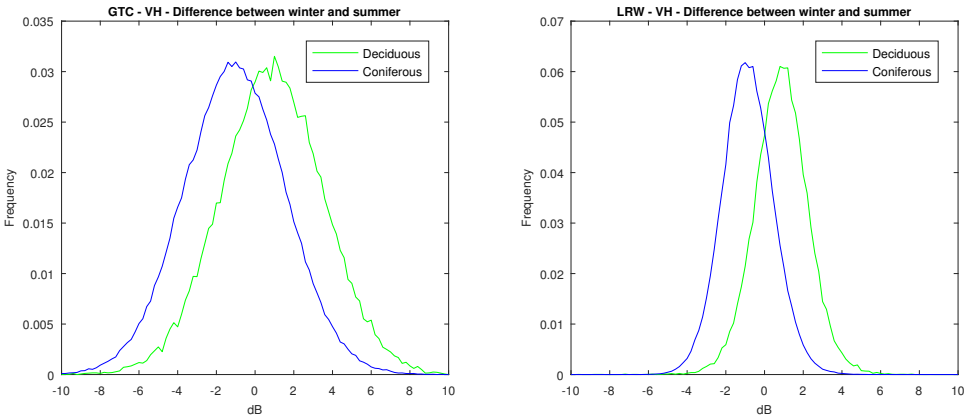

Figure 2.8: Histograms of the difference between winter and summer VH backscatter of the two forest types for the GTC images (left) and the LRW composites (right). n = 36621 for deciduous forest, 152930 for coniferous forest.

2.3.2 Time series analysis of LRW composites

The temporal evolution of the spatial descriptors is shown in Figure 2.9. Inspecting the LRW composite time series, the same features as in section 2.3.1 were observed. In addition to the spatial descriptors, temporal descriptors were calculated for the approximately 70 LRW composites. Examining these plots, the seasonal behaviour of the backscatter of the different species becomes even more apparent. An influence of temperature on the backscatter is seen at both polarisations and for all three species. This is manifested in minor changes in summer and major changes in winter, when temperatures were below the freezing point. The variance of the backscatter per composite was stable over time. The band between the 25 & 75% percentiles measured consistently approximately 1.5 dB for all species and study areas. Only for the study areas in ZH (Figure 2.9 a, c - e) the band became broader in summer 2015 due to the fewer S-1 acquisitions available in that period.

The temporal descriptors for all the study areas are summarised in Table 2.5 for VH and Table 2.6 for VV polarisation. For the beech stands with available phenological ground observations and the two oak stands, Table 2.7 compares the extracted break dates from the VH polarisation time series with the reported leaf emergence and fall.

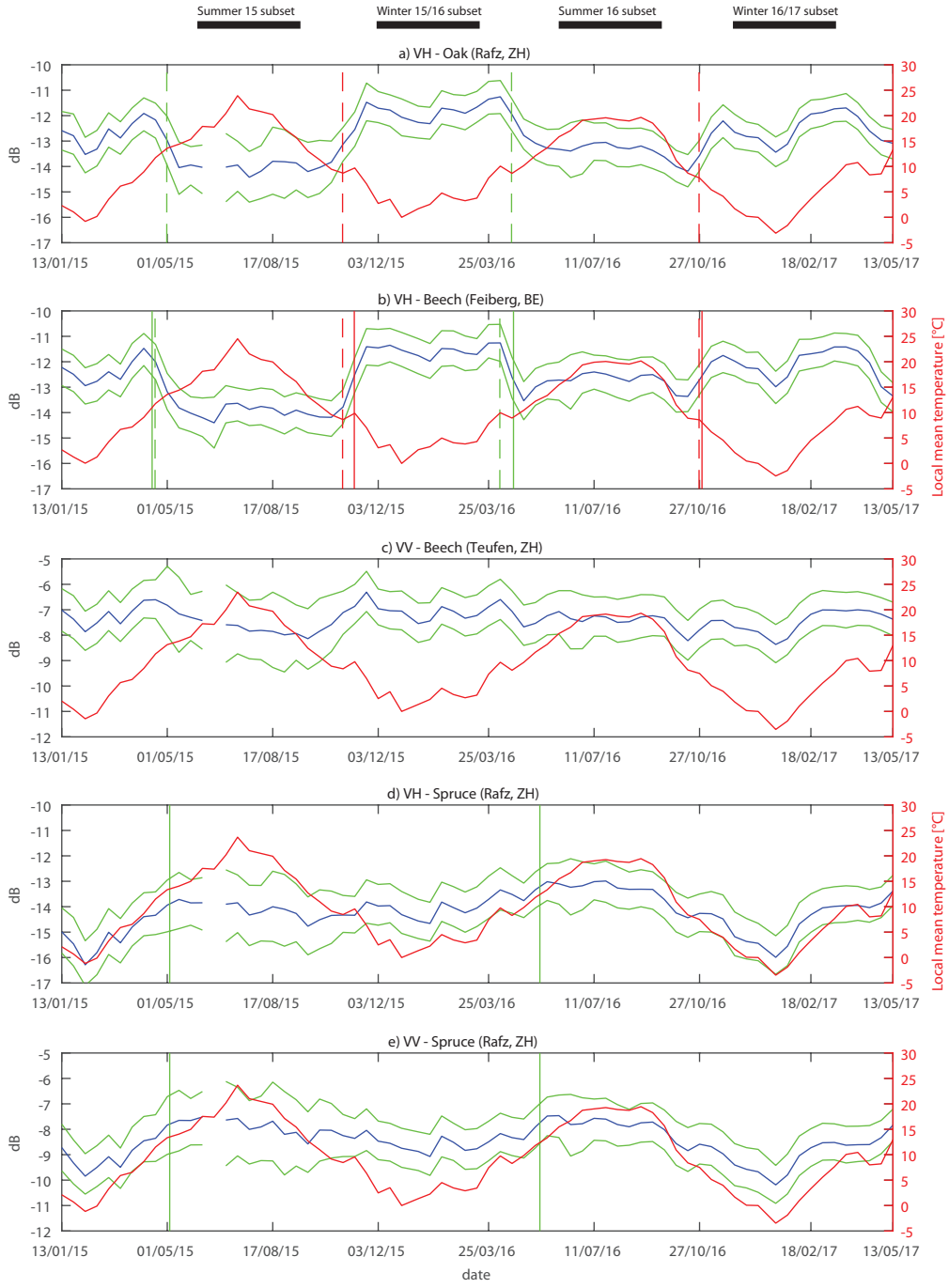

Figure 2.9: Temporal plots of species backscatter from LRW composites for selected study areas. Blue shows the median, green corresponds to the 25 & 75% percentiles. In red, the mean temperature for the 24 day period corresponding to each LRW composite. The solid vertical lines show phenological ground observations. Vertical green lines indicate leaf emergence for beech, and needle shoot for spruce. Red lines show the leaf fall date for beech. Dashed lines correspond to the backscatter derived break dates. The black bars on top of the figure display the periods used for the calculation of winter (01/12 - 15/03) and summer (01/06 - 15/09) medians.

2.3.2.1 Deciduous species (beech and oak)

Figure 2.9 shows that at VH polarisation, areas with deciduous species followed distinctive seasonal backscatter patterns. Backscatter was higher during leaf-off and lower during leaf-on conditions. For beech, the backscatter median ranged between -13.05 and -12.54 dB over the whole time series for the different study areas. The medians of winter and summer varied substantially between the two investigated years. Backscatter in winter was higher, with higher values observed in winter 2015/16 than winter 2016/17 (Table 2.5). Backscatter in summer was lower, with higher medians observed for the year 2016 (see 2016/17 in Table 2.5). Hence, the δs between winter and summer medians also differed between the years. For 2015/16, they ranged from 1.61 to 2.33 dB, whereas for 2016/17 the difference was between -0.49 and 0.65 dB. Most δs were positive, giving a clear indication of the higher backscatter in winter. Only study area 1 had a negative δ in 2016/17, caused by significantly lower backscatter due to temperatures below the freezing point in winter 2017 (see Figure 2.9 a).

Table 2.5: VH polarisation time series descriptors for the five study areas (SA) with their respective occurring species (S). Column N shows the number of LRW composites and $\bar{P}x$ the mean number of processed pixels. $\tilde{x}$To, Q1To and Q3To are the median, 25 & 75% percentiles over the whole time series. $\tilde{\gamma}^0_{win}$, $\tilde{\gamma}^0_{sum}$ and δ show the medians for winter, summer and the difference between the two. These descriptors were calculated for the years 2015/16 and 2016/17. The displayed backscatter values are in dB.

							2015/16			**2016/17**		
SA	**S**	**N**	$\bar{P}x$	$\tilde{x}$**To**	**Q1To**	**Q3To**	$\tilde{\gamma}^0_{win}$	$\tilde{\gamma}^0_{sum}$	δ	$\tilde{\gamma}^0_{win}$	$\tilde{\gamma}^0_{sum}$	δ
1	Sp	72	2303	**-14.08**	-15.00	-13.22	-14.28	-14.10	**-0.18**	-15.40	-13.25	**-2.15**
2	Sp	72	4583	**-14.02**	-15.00	-13.09	-14.03	-13.96	**-0.07**	-15.01	-13.11	**-1.90**
1	Be	72	1348	**-13.05**	-13.87	-12.24	-12.53	-14.14	**1.61**	-13.37	-12.88	**-0.49**
2	Be	72	1569	**-12.69**	-13.48	-11.83	-11.80	-13.76	**1.97**	-12.61	-12.82	**0.21**
3	Be	73	757	**-12.58**	-13.35	-11.87	-11.67	-14.00	**2.33**	-12.12	-12.77	**0.65**
4	Be	73	1271	**-12.54**	-13.23	-11.82	-11.56	-13.87	**2.31**	-12.23	-12.54	**0.30**
1	Oa	72	1485	**-12.97**	-13.62	-12.26	-11.98	-13.94	**1.96**	-12.84	-13.23	**0.38**
5	Oa	73	639	**-13.09**	-13.71	-12.51	-12.17	-13.62	**1.45**	-12.64	-13.24	**0.60**

Compared with beech, the two oak stands showed slightly lower median backscatter over the whole times series with values of -12.97 and -13.09 dB. The winter and summer medians of both years did not differ significantly from the values observed for beech. δ values of 1.96 and 1.45 dB for 2015/16 and 0.38 and 0.60 dB for 2016/17 were observed. As for beech, this δ was positive for both oak stands in both years, indicating a seasonal change in backscatter with higher values in winter.

Table 2.6: VV polarisation time series descriptors for the five study areas (SA) with their respective occurring species (S). Column N shows the number of LRW composites and $\bar{Px}$ the mean number of processed pixels. $\tilde{x}$To, Q1To and Q3To are the median, 25 & 75% percentiles over the whole time series. $\tilde{\gamma}^0_{win}$, $\tilde{\gamma}^0_{sum}$ and δ show the medians for winter, summer and the difference between the two. These descriptors were calculated for the years 2015/16 and 2016/17. The displayed backscatter values are in dB.

							2015/16			**2016/17**		
SA	**S**	**N**	$\bar{Px}$	$\tilde{x}$**To**	**Q1To**	**Q3To**	$\tilde{\gamma}^0_{win}$	$\tilde{\gamma}^0_{sum}$	δ	$\tilde{\gamma}^0_{win}$	$\tilde{\gamma}^0_{sum}$	δ
1	Sp	72	2303	**-8.46**	-9.25	-7.62	-8.72	-7.91	**-0.81**	-9.62	-7.76	**-1.86**
2	Sp	72	4585	**-8.46**	-9.39	-7.59	-8.68	-7.95	**-0.74**	-9.52	-7.75	**-1.78**
1	Be	72	1348	**-7.75**	-8.54	-6.98	-7.73	-8.23	**0.51**	-8.43	-7.49	**-0.93**
2	Be	72	1569	**-7.34**	-8.14	-6.41	-7.22	-7.83	**0.61**	-7.77	-7.28	**-0.48**
3	Be	73	757	**-7.07**	-7.86	-6.38	-6.85	-7.44	**0.59**	-7.28	-7.08	**-0.20**
4	Be	73	1271	**-7.11**	-7.83	-6.34	-6.92	-7.37	**0.44**	-7.28	-6.85	**-0.43**
1	Oa	72	1485	**-7.45**	-8.13	-6.71	-7.13	-7.89	**0.76**	-7.98	-7.60	**-0.38**
5	Oa	73	639	**-7.70**	-8.26	-7.15	-7.79	-7.43	**-0.36**	-7.98	-7.63	**-0.35**

Comparison of the break dates and their respective ground observations for the years 2015 and 2016 for the different beech and oak stands (Table 2.7 and Figure 2.9 b) shows that they match approximately with the reported leaf emergence and fall. For most study areas, the differences between the break dates and the observations were within or close to the uncertainty (± 12 days) caused by the temporal resolution of the LRW composites. In 2015, the first break dates were predicted between 3 and 11 days later compared to the leaf emergence, while in 2016, they were predicted between 14 days in advance and 5 days later.

For two study areas, the extraction of the break dates did not work very well in one year. For beech in Rafz in 2016, the second break date seems to represent the leaf emergence, as the first break date was too early for leaf emergence. For oak in Büren a.d.A. in 2015, the first break date appeared far too late (approximately 80 days) for recording leaf emergence.

The second break date, however, captured the leaf fall even better than the first the leaf emergence. In 2015, the break dates were predicted between 12 days in advance and 1 day later, while in 2016, they were predicted 3 days in advance. Visually these results are depicted with the vertical lines in the temporal plots in Figure 2.9. The predicted first break dates for the oak stands are also noteworthy. They had a tendency to be a few days later than the beech stands in the same study area (Rafz) or nearby (Büren a.d.A. to

Galsberg/Feiberg).

Table 2.7: Comparison of the break dates (BD) extracted from the VH polarisation time series with the respective leaf emergence (LE) and leaf fall (LF) ground observation for the different study areas. For both years, the values are displayed in day of the year. The listed uncertainty is due to the compositing timespan of 24 days.

		2015				2016			
Study area	**Species**	**BD1**	**LE**	**BD2**	**LF**	**BD1**	**LE**	**BD2**	**LF**
Rafz (ZH)	Beech	121±12	110	301±12	300	61±12	104	109±12	308
Galsberg (BE)	Beech	109±12	106	301±12	313	97±12	111	301±12	304
Feiberg (BE)	Beech	109±12	106	301±12	313	97±12	111	301±12	304
Rafz (ZH)	Oak	121±12	-	301±12	-	109±12	-	301±12	-
Büren a.d.A. (BE)	Oak	205±12	-	313±12	-	121±12	-	313±12	-

In VV polarisation, the backscatter of both deciduous species was higher than at VH polarisation with a median over the whole time series ranging between -7.75 and -7.07 dB. No distinctive seasonal pattern was observed. But looking at the plotted time series of the beech stand in Teufen (Figure 2.9 c), after a short increase in spring, a gradual decrease in backscatter from about -6.7 to -8 dB in summer was observed in both years.

2.3.2.2 Spruce

Spruce forests exhibited seasonal backscatter behaviour in both polarisations. However, compared to the deciduous species, the behaviour was inverted. Higher backscatter was recorded in summer, and lower backscatter in winter. Generally, the spruce stands showed lower backscatter of about 1 dB compared to the deciduous species. This was consistently shown in the median backscatter values over the whole time series. In VH, the two stands had a median of -14.08 and -14.02 dB, where as in VV, their median was -8.46 dB.

As for the deciduous species, the medians of winter and summer varied across the two years. In winter, VH backscatter was lower than in summer. Lower backscatter was observed in winter 2016/17 than in winter 2015/16 (Table 2.5). In summer, backscatter was generally higher. In summer 2016, higher values were observed than in summer 2015 (for 2016 see 2016/17 in Table 2.5). In VV, backscatter differences between winter and summer and the two years followed similar patterns (Table 2.6). This led to negative δ values at both polarisations. Compared with VH, the δ values were higher at VV. Hence, the seasonal difference was higher in VV. This can be seen in Figure 2.9 d) and e), where the seasonal difference in backscatter appears slightly higher in VV than in VH.

2.3.3 Classification performances

The demonstrated differences in backscatter between the different species was next used to classify independent validation data into forest classes. Table 2.8 presents the performance of the *forest type* classification. Table 2.9 shows the performance of the *species* classification. The first two columns in both tables list the number of pixels used in the training and validation sets. The classification performance was assessed using the accuracy values in the following columns.

Table 2.8: Classification result for the two forest types. The mean number of pixels used for training and validation in the RF classification for the classes deciduous and coniferous forest are listed with the mean producer's accuracy (PA), user's accuracy (UA), overall accuracy (OA) and Cohen's κ of the 40 different RF models.

Forest class	**Training**	**Validation**	**PA**	**UA**	**OA**	κ
Deciduous	20006	9077	0.84	0.88	0.86	0.73
Coniferous	19982	8729	0.88	0.84		

For both forest classes, producer's and user's accuracies were fairly high, resulting in a high overall accuracy and a high Cohen's κ (Table 2.8). The predictors' importance listed in Figure 2.10 showed that all twelve predictors contributed to the achieved classification result. No single predictor appeared to dominate.

Table 2.9: Classification result for the three different species. The mean number of pixels used for training and validation in the RF classification for the three species are listed with the mean producer's accuracy (PA), user's accuracy (UA), overall accuracy (OA) and Cohen's κ of the 40 different RF models.

Species class	**Training**	**Validation**	**PA**	**UA**	**OA**	κ
Beech	2003	922	0.56	0.62		
Oak	1995	993	0.70	0.68	0.72	0.58
Spruce	2004	981	0.88	0.83		

As expected, compared with the *forest type* classification, the achieved performance was lower for the *species* classification (Table 2.9). This was mainly caused by confusion between beech and oak, resulting in lower PA and UA for both classes. The performance for spruce, however, was virtually the same as for coniferous forests. Due to the limited availability of oak forests in the Canton of ZH, the number of training and validation pixels

was much lower for the *species* classification compared with the *forest type* classification. For the *species* classification, the importance of the predictors was not as consistent as in the *forest type* classification (Figure 2.10). The δ of the year 2016 of both polarisations, but especially VH, was very important. The break dates of 2015 played a subordinate role.

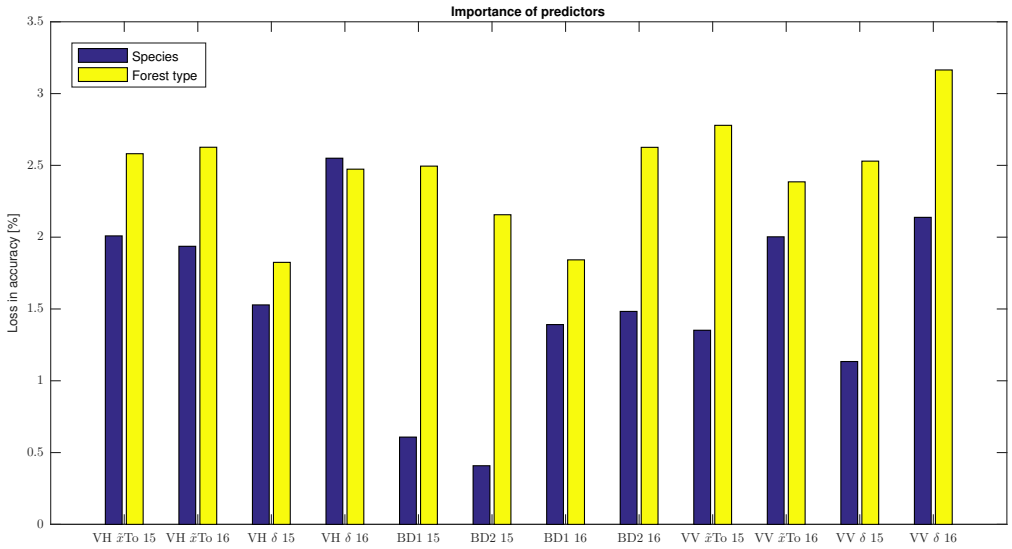

Figure 2.10: Importance of individual predictors in the two classifications. The predictors are the total annual medians ($\tilde{x}$To) and δs of the two years for the two polarisations. The break dates (BD) extracted from the VH time series for both years complete the set of predictors.

2.4 Discussion

Analysis of the SAR C-band backscatter time series of forests showed that the observed backscatter behaviour was robust for multiple sites over multiple years. Generally, annual median backscatter of forests consisting of deciduous species was higher than backscatter of forests consisting of spruce. Both types of forests showed distinctive seasonal backscatter patterns. The deciduous species had higher backscatter in winter and lower in summer, while spruce exhibited the opposite behaviour.

Temporal variation in SAR data is caused by signal noise and short- and long-term environmental changes. The former two were strongly mitigated because of the methodology used in the SAR data processing. The LRW approach combines several acquisitions into one composite. Hence, the approach suppresses the influences of signal noise and short-

term variations, such as rainfall events before single acquisitions. As a result, the annual variation can mainly be attributed to long-term environmental changes occurring within the study areas. Moreover, the decision to use terrain-flattened RTC images could contribute to better results as well. All study areas (bar Büren a.d.A.) investigated in this study are in hilly terrain.

2.4.1 Seasonal signature of deciduous species

Both deciduous species showed seasonal changes in VH backscatter behaviour. Backscatter values dropped in the spring from a high winter level to a low summer level, rising again in the autumn, resulting in positive δ values. The predominant long-term change in deciduous forests is the seasonal vegetation cycle, manifested in the annual growth of trees and presence of foliage. The presence of foliage occurred at the time with the lower backscatter values observed in the summer months: a dependence of the backscatter on leaf presence was observed (Proisy et al., 2000; Dostálová et al., 2016).

Potential causes for the changing cross-pol scattering behaviour remain uncertain. One reason might be the changing size of the scatterers present in the tree crown. In summer, leaves substitute branches as main scatterers. C-band is primarily sensitive to small branches and only secondarily to leaves (Chauhan et al., 1991). Leaves have been reported to act not only as scatterers but also as attenuators for C-band (Leckie & Ranson, 1998; Kovacs et al., 2013). Hence, leaf emergence in spring leads to a combination of effects, resulting in lower backscatter during the leaf-on period. (a) A scatterer substitution, where the sensitivity of C-band is reduced and (b) an attenuation of the microwave energy by the leaves. Leaf fall in autumn otherwise exposes the small branches again, leading to higher backscatter.

Another possible reason for higher backscatter values during the leaf-off period is the influence of ground scattering (Wegmüller et al., 1994). With lower attenuation in winter than in summer, ground scattering contributes stronger to the measured backscatter. Proisy et al. (2000) showed that in winter, the contribution of soil and branches were comparable, whereas in summer, the contribution of the soil dropped because of the attenuation by the leaves.

Surprisingly, VV backscatter did not show the same seasonal behaviour as VH. Although slightly higher backscatter was observed in winter, the δs show that there was a less defined seasonal signature. An interesting feature was the constant decrease in backscatter

during the leaf-on season. This could be attributed to the slow drying of leaves in summer (Mougin et al., 1998).

Leckie & Ranson (1998) did not mention a difference in temporal signature between VH and VV backscatter in their comprehensive review of SAR backscatter of forest. Potential reasons for our observed differences between the two polarisations are discussed in the following. Volume scattering becomes more important when the scatterers present are more random and complex (Bush et al., 1976). Volume scattering is also known to have a larger influence on VH than VV polarisation (Leckie & Ranson, 1998; Solimini, 2016). Leaf emergence probably leads to a more complex arrangement of the scatterers, leading to a stronger influence on the VH than the VV backscatter. Our empirical observation of the difference between leaf-off and leaf-on conditions in C-band backscatter of deciduous forests corresponded well with the simulation made by Chuah & Tan (1992). The S-1 IW acquisitions processed in our study were measured at incident angles between $31°$ and $46°$. Their modelled C-band absolute backscatter values at $50°$ incident angle were different at both polarisations, but they also showed a positive difference at VH and almost no difference at VV between leaf-off and leaf-on conditions.

2.4.2 Break date extraction to monitor phenology

The break date extraction yielded promising predictions, bearing in mind that the time series had a temporal resolution of 24 days. Even finer details such as differences between species were observable. The observed tendency of the oak stands to have their leaves emerge later than the beech stands agrees with the common theory concerning the timing of leaf emergence of the two species (Lange et al., 2016). However, it is important to consider that the independent ground validation data was produced by observations from volunteers. Hence, the reported values have to be treated with caution.

We showed that with our approach, the phenological cycles of deciduous forests can be monitored on a landscape scale. With longer time series available in the future, it will be possible to analyse phenology trends with S-1 data. The same type of phenology trend analyses that have usually used MODIS Normalised Difference Vegetation Index (NDVI) such as White et al. (2009) in North America or Hamunyela et al. (2013) in Europe could be conducted. Using S-1 instead of MODIS data, an enhanced spatial and temporal resolution would be available.

The results also showed that there are still some issues using the *breakpoints* algorithm for the extraction of the break dates. The problems encountered for the two study ar-

eas can be explained by the weak dependency of the backscatter on foliage within each respective year. Other influences (e.g. exceptional freezing temperature) on the backscatter seemed to disturb the seasonal signature to such an extent that a smooth break date extraction was not always possible.

2.4.3 Seasonal signature of spruce

Backscatter from spruce stands did not show similar abrupt changes. At both polarisations, their seasonal signature were less pronounced and more gradual. Lower values were observed in winter and higher in summer, resulting in negative δ values. Because of their perpetual foliage, no strong influence of changing foliage or ground scattering was expected (Ahern et al., 1993). The backscatter of coniferous forests is mainly dependent on the number of needles and small branches (Dobson et al., 1992). Because the leaf area index (LAI) of coniferous forests is usually highest in July (Mougin et al., 1998), the highest backscatter can therefore be expected in that month. Dostálová et al. (2016) argued that in addition to the larger number of needles, the development of the understory in summer might also influence backscatter in coniferous forests.

The observed lower annual VH median backscatter of spruce stands compared to beech and oak stands was mainly due to the higher backscatter observed in winter for the latter, caused by the factors mentioned in section 2.4.1. At VV, this effect was not observed to the same extent. Nevertheless, higher backscatter in winter relative to the spruce stands was apparent. This observation confirms previous studies that investigated differences in backscatter between deciduous and coniferous species (Drieman et al., 1989; Ahern et al., 1993; Proisy et al., 2000).

2.4.4 Differences between the investigated years

Clear differences were observed within the timespan investigated. Inter-annual differences were most probably due to different meteorological conditions. A clear influence of temperature on the backscatter can be seen in Figure 2.9. In summer, higher VH backscatter was observed when temperatures were also higher. In winter, there was an even stronger influence of the temperature. When the temperature fell below the freezing point, the backscatter dropped significantly. This was mainly observed in January 2017, when temperatures in Switzerland were very low for a long period, but also in January 2015. Temperature is known to influence the dielectric properties of the scatterers (Olesk et al., 2015). Especially when temperatures are below 0 °C, dielectric properties of the

frozen scatterers change fundamentally, resulting in lower backscatter (Wegmüller et al., 1994).

Disparities were observed in the typical summer backscatter reductions of the deciduous forests at VH. Compared to 2016, the drop in 2015 was larger, which is well depicted in the plot of the study area Feiberg (Figure 2.9 b). This can probably be attributed to different weather conditions in the springs and summers of 2015 and 2016. Compared to 2016, temperatures, sunshine duration and the amount of precipitation in the study areas in spring 2015 were higher than normal (Federal Office of Meteorology and Climatology MeteoSwiss, 2015, 2016). These favourable growing conditions might have caused a better development of the tree crowns for the deciduous species (Bequet et al., 2011). According to the points mentioned in section 2.4.1, a well developed crown with a high LAI would lead to a higher attenuation of the microwave energy. Thus, a larger drop would be expected and was observed.

Although precipitation can have an influence on backscatter (Sharma et al., 2005), no strong influence on short-term backscatter changes was detected in our data. As mentioned above, only a general influence on the growing season coupled with other meteorological factors was observed. This may be due to the applied compositing approach, which mitigates variations caused by short-term precipitation events.

Last, a possible influence of the absolute backscatter calibration issue in summer 2015 cannot be disregarded. To correct the wrong backscatter values, a simple correction was executed by subtracting a fixed value in the affected images (Miranda, 2015; El Hajj et al., 2016). Residual errors may have been larger in these earlier data, contributing to the differences between summer 2015 and summer 2016. But the observed disparities were not the same for the different study areas and caused no ”step” in the VV data, so the likelihood of radiometric miscalibration appears negligible.

2.4.5 Comparisons to other studies

The results of this study do not contradict previously published results but extend it with an unprecedented set of C-band cross-pol observations of mixed temperate forests. Similar backscatter values were retrieved in a simulation study of sensitivity of ERS-1 C-band VV backscatter over forest (Wegmüller et al., 1994). The non linear dependence of backscatter on temperature below the freezing point had also been simulated in that study. Proisy et al. (2000) analysed ERS-1/2 C-band VV backscatter of a mixed temperate forest for the timespan between April 1994 and February 1997. They presented similar VV

backscatter ranges from deciduous and coniferous stands. Their time series consisted of one image per month and had no VH measurements. Although they used a lower temporal resolution, the shape of their temporal backscatter plot of a beech stand throughout the year was similar to the one showed in this study. A recent study, analysing intra-annual S-1 data of an Austrian mixed temperate forest between February 2015 and 2016, yielded results that were in line with ours (Dostálová et al., 2016). The ranges of backscatter observed from deciduous and coniferous forests at VV and VH as well as the seasonal signatures shown by the two forest types at both polarisations were consistent.

2.4.6 Classification of forest types and species

The classification results show that the observed backscatter behaviour allows segmentation into two different forest types or even into three different species. Not only the VH data but also VV contributed to achieving the good classification performances. This was surprising, as the seasonal backscatter behaviour of deciduous forests was less distinct at VV than at VH polarisation.

As expected, accuracies were lower when classifying *species* vs. *forest type*. Substantial confusion was seen between the beech and oak class, whereas in the *forest type* classification, they are both part of the deciduous class. The accuracies for spruce, however, were almost the same as for the coniferous class. This was not surprising as the coniferous class is mainly composed of spruce. The high accuracies were reached due to the backscatter behaviour of spruce being substantially different to that of the two deciduous species. Spruce was also the only coniferous species that could be examined. Future studies might include more species and try to use their seasonal backscatter patterns for classification approaches.

In this study, only stands with species homogeneity higher than 80% were considered for the classification. Hence, it remains unclear how the classifiers perform on more heterogenous mixed forests. Future studies could test how the classifiers perform in mixed forests. However, when we compared the classification results to aerial images, we observed that the classifier was able to detect single spruce trees within a deciduous stand. Therefore, the classifiers might even outperform the aggregated forest stand-based independent ground reference. With a sampling interval of 10 m, the classifiers almost operate on a single tree level, whereas the information of the ground reference is based on larger areal extents. So, many misclassifications may have been caused by the nature of the

independent ground reference information. This might be verified in the future using a different ground reference with a higher spatial resolution.

There was a significant time difference between the ground reference and the SAR data acquisition. The ground reference was produced in 2010, so a considerable time gap of at least 5 years was a further possible source of errors. Logging activities during that period likely degraded the classification performance. Clear-cut logged spruce areas tended to be classified as deciduous, most probably due to the high ground backscatter.

It is difficult to perform an in-depth comparison to other approaches using SAR but also different remote sensing technologies to classify mixed temperate forests. Study areas, the species investigated, number of training and number of validation samples differed substantially between the studies. Nevertheless, our achieved accuracies were comparable to other studies classifying deciduous and coniferous forests using even fully polarimetric C-band SAR data (Rignot et al., 1994; Aghabalaei et al., 2016). Compared with other technologies such as airborne laser scanning (OA of 93% and $\kappa = 0.61$) (Bruggisser et al., 2017) or imaging spectrometer data (OA of 83% and $\kappa = 0.73$) (Roth et al., 2015), our *forest type* classification performance (OA of 86% and $\kappa = 0.73$) was also competitive.

2.4.7 Implications of the findings

If one is aware of the mentioned different influences on C-band backscatter, C-band data can be used for several applications. Its potential for the classification of mixed temperate forests has been presented. Thus, a repetitive classification of an area allows change detection over time. For ecological applications such as seasonal vegetation cycle monitoring, the use of C-band data will become progressively more interesting, as longer time series of data become available. Nevertheless, the capability of the data to observe subtle differences between the years has been shown using only 2.5 years of data. Because the production of S-1 data is promised until at least 2030 (Berger et al., 2012), longer time series of data should be available in the future. Using them, changes over time, such as the shift of phenophases due to climate change, could be detected and quantified.

Compared with state-of-the-art methods using optical data, SAR has valuable advantages. The sensitivity to structural elements adds an additional independent dimension of information about forests. This structural information helps to improve the understanding of natural processes in forests. Furthermore, the high temporal and spatial resolution offered by Sentinel-1 allows a much denser sampling of data. Since the end of the commissioning phase of Sentinel-1B in September 2016 (Schubert et al., 2017), the number of

products is high enough to generate LRW composites with over twice the temporal resolution than that used in this study. A LRW composite every six days would offer even more insights into the temporal evolution of the backscatter of forests. To further enhance the temporal resolution, efforts should be made to combine S-1 and RADARSAT Constellation Mission data, due for launch in 2018 (de Lisle & Iris, 2016).

With high temporal resolution available, there lies also great potential in analysing larger spatial extents. The backscatter behaviour of forests described in this study was also observed over the whole Alpine region (Lat/Lon: 43.5 - 49°N / 5.5 - 17.5°E). Applying the same methodology as described in section 2.2.3 but with a temporal resolution of the LRW composites of 12 days, descriptors were calculated within the Coordination of Information on the Environment (CORINE) land cover classes for deciduous and coniferous forest (Copernicus, 2016). Plotted in the temporal domain, the same seasonal patterns are apparent at both polarisations and for both forest types, as shown in Figure 2.11.

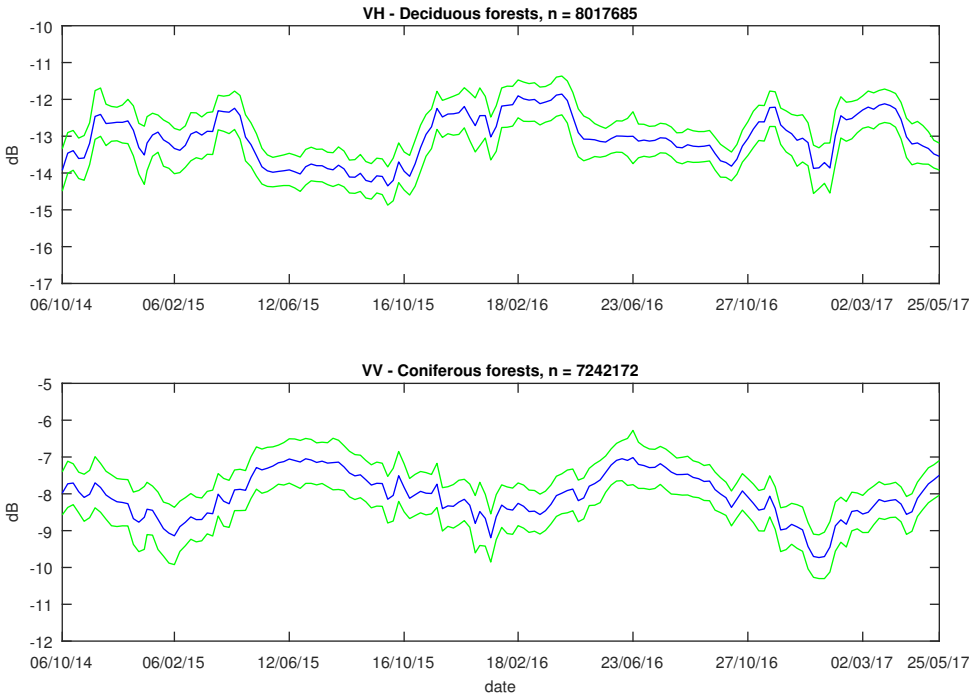

Figure 2.11: Temporal plots of the per LRW composite calculated spatial descriptors median (blue), 25 & 75% percentiles (green) for decidous and coniferous forests of the Alpine region (Lat/Lon: 43.5 - 49°N / 5.5 - 17.5°E). The temporal resolution of the LRWs was 12 days and the time period depicted ranges from October 2014 to May 2017. The number of investigated pixels (n) was comparable for both forest types.

Future research could focus on more detailed analysis of the backscatter and the understanding of scattering processes. An in-depth study of the observed summer drop in VH backscatter might result in interesting new insights, especially with a higher temporal resolution. Differences, for example, between the deciduous species are hypothesized, but could not be tested in this study. A dependence of the magnitude of the observed drop to LAI could also be tested. If the drop in backscatter is caused by the attenuation of the leaves, a dependence is credible. This could be tested by correlating VH backscatter time series with periodic LAI estimations derived from hemispherical images of deciduous forest stands in spring or autumn (Chianucci & Cutini, 2013).

This leads to the question to what extent the findings of this study could be transferred to other ecosystems for time series analysis. In tropical or boreal ecosystems, where the use of SAR data is already well established, the use of multitemporal C-band data might contribute valuable new insights into the temporal evolution of these ecosystems.

2.5 Conclusions

This study showed that multitemporal C-band absolute backscatter data has the potential to complement or supplement optical remote sensing data for use in forest mapping or ecological applications. Forests consisting of broad-leaved, deciduous species, such as beech and oak, produce stronger backscatter in both polarisations than forests consisting of spruce. Typical seasonal phenology signatures were also observed within forested areas. In VH, areas consisting of deciduous forests showed a consistent and distinct intra-annual backscatter pattern with higher backscatter in winter and lower in summer. In coniferous forests, however, the opposite behaviour with lower backscatter in winter and higher in summer was observed. The same behaviour, but even more distinctive, was observed in coniferous forests at VV, whereas deciduous forests showed almost no seasonal cycle in VV.

These temporal signatures simplify the classification of temperate mixed forests because of the striking differences between the temporal signatures of deciduous vs. coniferous forests. Good classification performances were achieved for the *forest types* (OA of 86% and $\kappa = 0.73$) and for three different *species* (OA of 72% and $\kappa = 0.58$). The strong seasonal signal in VH allows the monitoring of phenology of deciduous forests. The dates independently reported for leaf emergence and leaf fall of three different study areas were satisfyingly matched. Almost all extracted break dates were within the error margin

(± 12 days) of the available temporal sampling.

These findings show that using multitemporal C-band data offers several new possibilities. Periodic and cost-effective mapping of mixed temperate forests will ease forest management to a great extent. In the near future, longer time series of S-1 and RADARSAT Constellation Mission data over several years will be available with high temporal resolution. Using them, monitoring on different sets of spatial and temporal scales of different ecosystems will be possible. Results of these might lead to interesting ecological insights, such as an assessment of the shift of phenophases or a quantification of changes in species composition due to climate change.

3 | Supplementary materials

3.1 Influence of the number of iterations on the classification

To retrieve representative classification performance measures, the RF classifications were iterated 100 times and mean measures were calculated after each iteration. Figure 3.1 shows the dependence of the overall accuracy on the number of iterations conducted for the *species* and the *forest type* classification. After investigation of these plots, 40 iterations was deemed to be enough to achieve representative measures. After 40, increasing the number of iterations did not significantly change the overall accuracy ($\pm 0.25\%$).

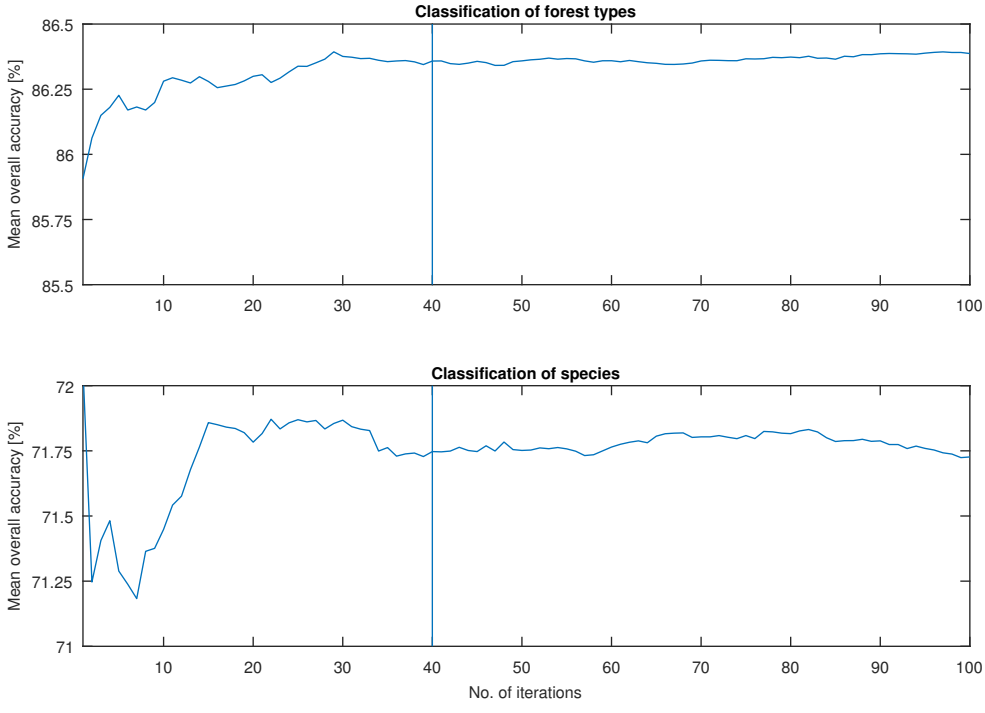

Figure 3.1: The mean overall accuracy shows a dependence on the number of classification iterations. The vertical line indicates the chosen number of iterations for both classifications.

3.2 Additional results using the aerial image forest stand map

3.2.1 Temporal plots of additional species

This section contains temporal plots of all available species in the aerial image forest stand map distributed over the Canton of Zurich. The methodology applied was the same as described in section 2.2.3. Homogeneity thresholds of 80% for all species were chosen. This led to scattered pixels of forest stands containing either the species European beech (*Fagus sylvatica*), oak (*Quercus robur, Quercus petraea*), Norway spruce (*Picea abies*), Silver fir (*Abies alba*), European larch (*Larix decidua*) or Scots pine (*Pinus sylvestris*). Figure 3.2 and Figure 3.3 display the temporal backscatter behaviour of the different species at VH and VV polarisation, respectively.

For the species investigated in chapter 2, we observed the same backscatter ranges and seasonal backscatter patterns on the larger scale of the whole canton as on the forest stand scale. Pines showed higher backscatter of about 1 dB at VH compared to the other coniferous species. Firs and pines exhibited similar temporal backscatter behaviour as spruce at both polarisations. Lower backscatter values were observed in winter and higher in summer. But the seasonal backscatter difference of pine was not as distinct as of spruce and fir at both polarisations. Interestingly, larches showed similar backscatter behaviour as the deciduous species at VH polarisation. In winter 2015/2016, higher backscatter values were seen, whereas in summer 2015 and 2016 backscatter was slightly lower. Hence, the seasonal cycles of deciduous larches could be observed in the same way as of the deciduous species beech and oak.

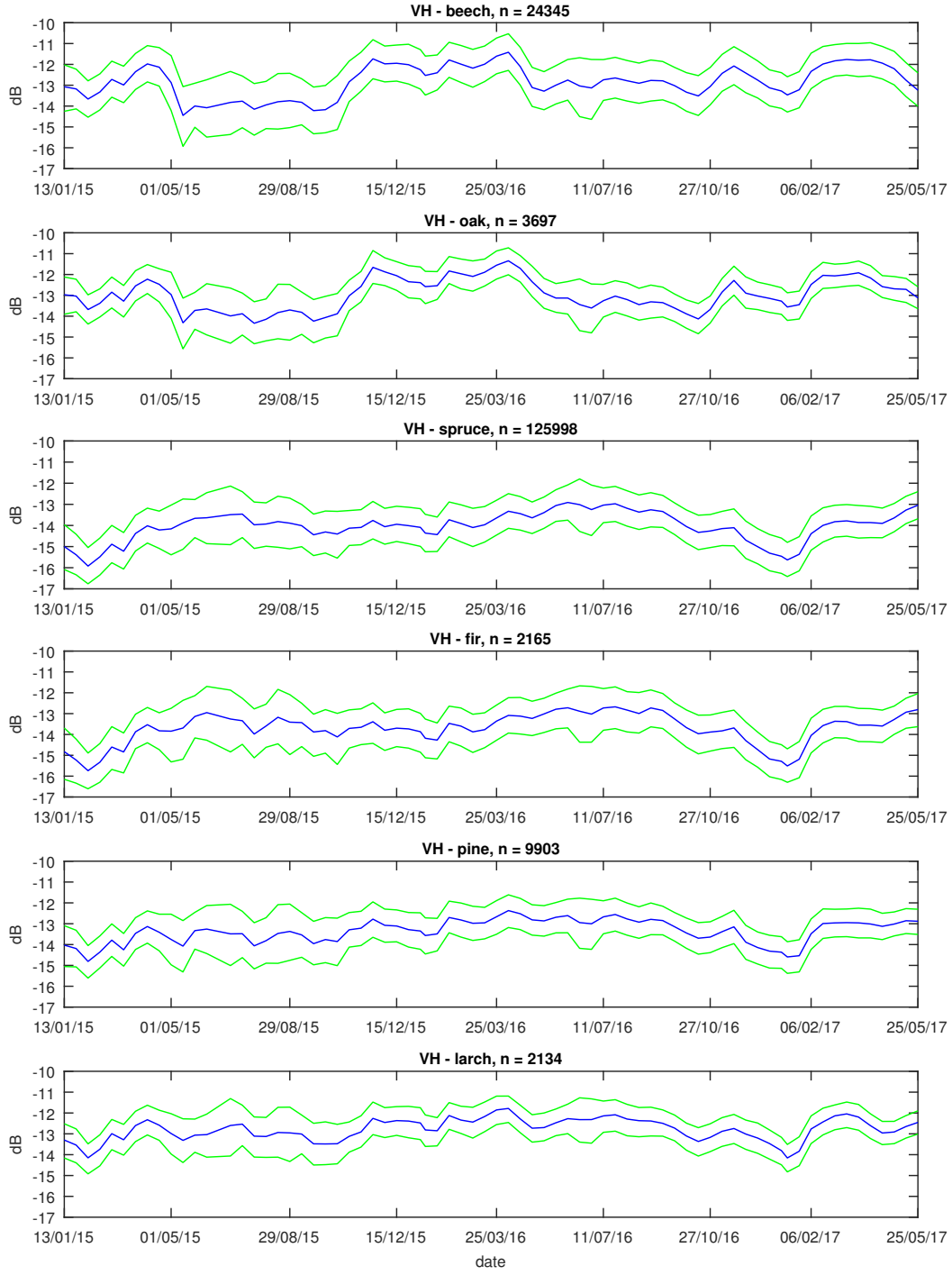

Figure 3.2: Temporal plots of LRW composite backscatter at VH polarisation for the different species. Blue shows the median, green corresponds to the 25 & 75% percentiles. The number of investigated pixels (n) varied greatly across species.

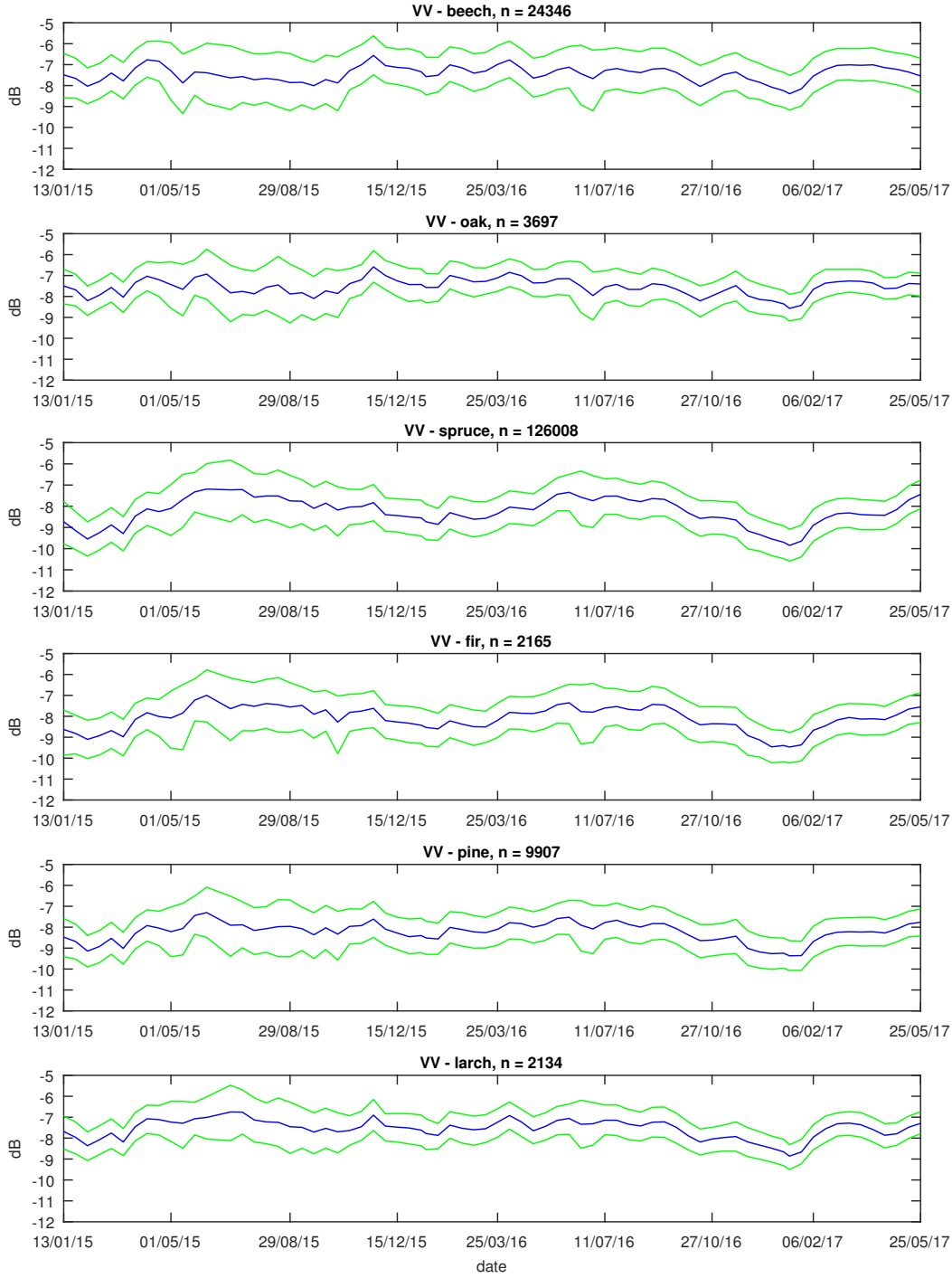

Figure 3.3: Temporal plots of LRW composite backscatter at VV polarisation for the different species. Blue shows the median, green corresponds to the 25 & 75% percentiles. The number of investigated pixels (n) varied greatly across species.

3.2.2 Classification with four species

A classification that included an additional species not investigated in chapter 2 was also conducted. Forest stands of three additional coniferous species (Silver fir, Scots pine and European larch) were available in the dataset of the aerial image forest stand map. But only the number of available pixels (n=9907) for pine was deemed to be high enough to be used in a classification. The classifier RF with the same parameters as described in section 2.2.3.5 was used. The classification was conducted in the same manner, using the twelve different predictors and splitting the available pixels into a balanced training and validation set. The classification performance is shown in Table 3.1.

Table 3.1: Classification result for the four species. The mean number of pixels used for training and validation in the RF classification for the four different classes are listed with the mean producer's accuracy (PA), user's accuracy (UA), overall accuracy (OA) and Cohen's κ of the 40 different RF models.

Species class	**Training**	**Validation**	**PA**	**UA**	**OA**	κ
Beech	1987	932	0.48	0.55	0.63	0.51
Oak	2005	993	0.68	0.63		
Spruce	2000	985	0.77	0.70		
Pine	2009	1016	0.59	0.63		

The performance of the classification (OA of 0.63 and κ = 0.51) was worse than with three species (see section 2.3.3 to compare). Producer's and user's accuracy were lower for all three species beech, oak and spruce. The PA (0.59) and UA (0.63) values of pine were in the same lower range as the ones of beech. Better performances were achieved for oak and spruce.

3.3 Plant area index calculation from within a deciduous forest stand

Hemispherical images were taken to enable an independent estimation of the changes occurring within a deciduous forest stand during leaf emergence. The images were taken with a NIKON D200 and the SIGMA EX DC f2.8 4.5 mm circular fisheye lens. The acquisitions were made in spring 2017 on 16/03, 01/04, 17/04 and 05/05 at the four locations listed in Table 3.2 within the study area of Rafz. One exemplary time series acquired is depicted in Figure 3.4. The four images show the course of the emergence of leaves for Oa1.

Table 3.2: The forest stands at the four locations in the study area mainly consisted of either beech or oak trees. Swiss map coordinates: CH1903+ / LV95.

Abbreviation	**Predominant species**	**Coordinates**
Be1	Beech	2'677'716.54, 1'272'147.59
Be2	Beech	2'678'113.29, 1'272'181.73
Oa1	Oak	2'678'923.96, 1'273'229.79
Oa2	Oak	2'679'512.05, 1'272'638.26

To quantify leaf emergence, the plant area index (PAI) was calculated on the four dates at the four different locations. The software CAN_EYE (V. 6.4.7) was used to calculate the PAI (Weiss & Baret, 2017). CAN_EYE classified the hemispherical images into sky or vegetation using an interactive threshold based classification approach. On the basis of this classification, CAN_EYE then calculated the PAI. The parameters listed in Table 3.3 were used to obtain the PAI values.

Table 3.3: CAN_EYE parameters used to obtain the PAI values.

Parameter	**Value**
Image size	Rows: 2592, Columns: 3872
Optical centre	Line: 1296, Column: 1936
Projection function	Polynomial order = 1, P1 = 0.1016; P1 = 90°/886 px (image radius in pixel)
Circle of interest	60° (default)
Sub sample factor	1 (default)
Zenith angular resolution	2.5° (default)
Azimuth angular resolution	2.5° (default)
FCover angular resolution	10° (default)
Clumping parameter	8 (default)

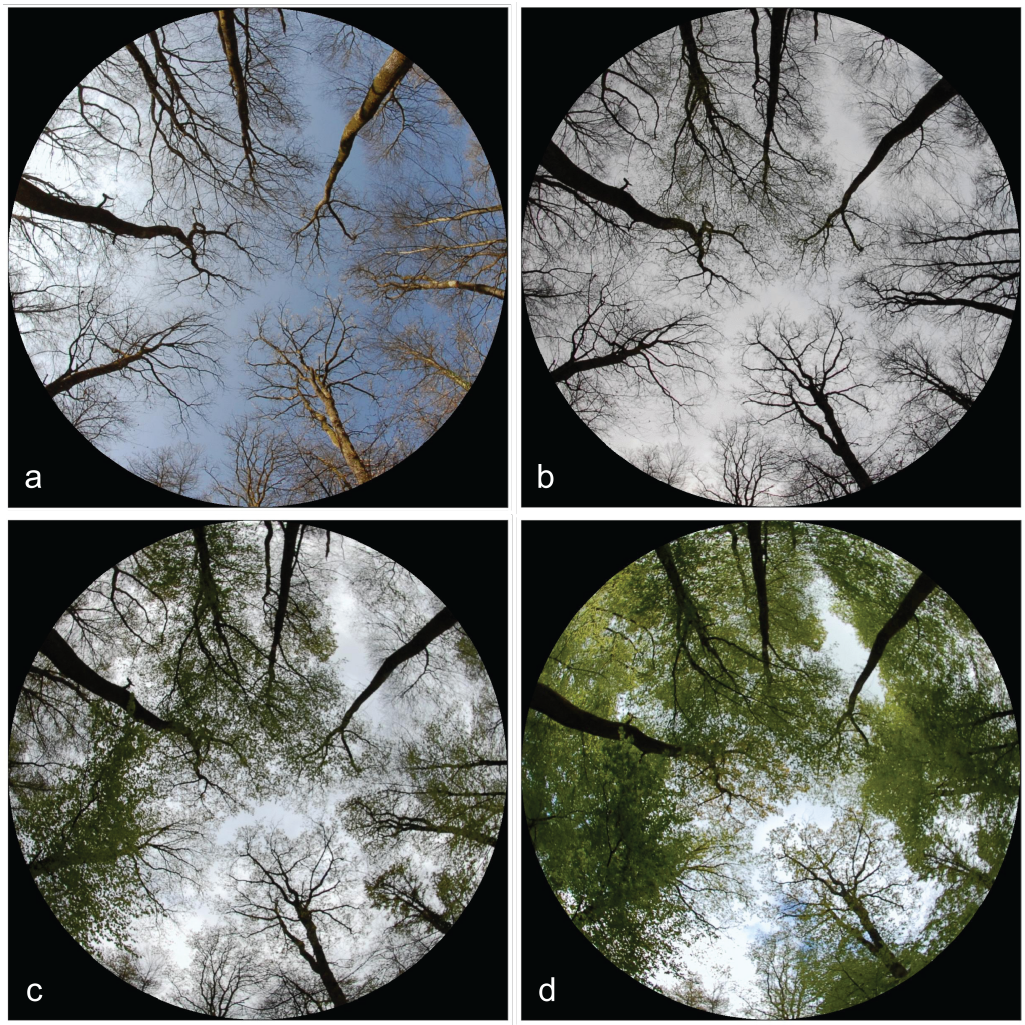

Figure 3.4: Hemispherical images at the location Oa1 on four different dates. The images were taken on 16/03 (a), 01/04 (b), 17/04 (c) and 05/05 (d). There were more leaves in the tree crowns later in spring.

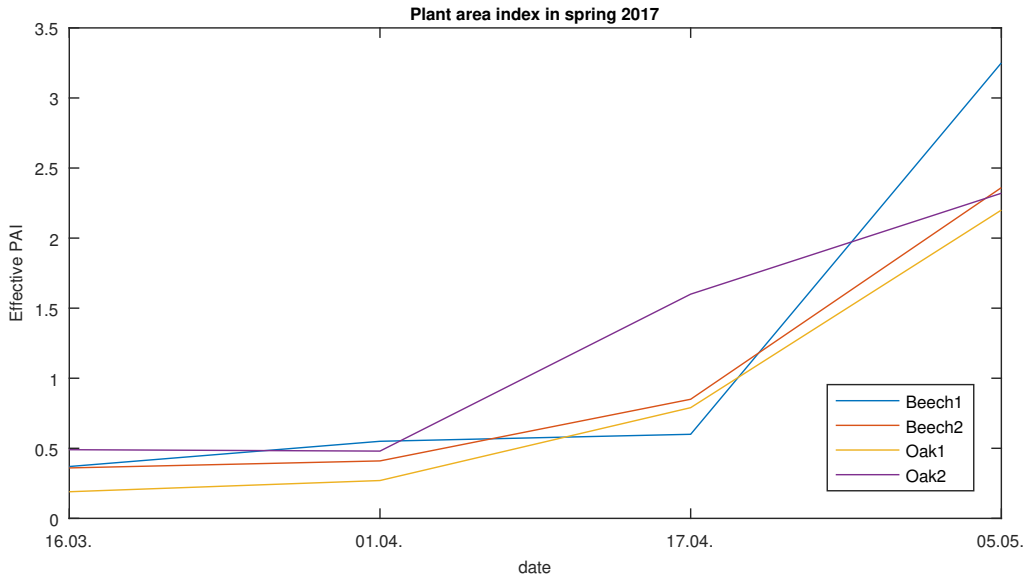

Figure 3.5: Evolution of the plant area index in spring. As observed in Figure 3.4, progressively in spring, higher effective PAI values were caused by the emergence of leaves. This observation was made at all four locations.

The obtained PAI values of the four different locations are shown in Figure 3.5. The values rose at all locations from the middle of March to the beginning of May. Investigating Figure 2.9 a), it can be observed that the PAI increase occurred at the time of decrease in VH backscatter. This affirmed the hypothesis that the decrease in VH backscatter is coupled to the emergence of leaves.

3.4 RGB-overlays containing the study areas

RGB-overlays of the Canton of Zurich and the northwestern part of the Canton of Bern were produced. The spatial extents of the two overlays correspond to those of the two close-ups of Figure 2.1. The study areas 1 and 2 are contained in Figure 3.6, whereas the study areas 3, 4 and 5 are included in Figure 3.7. Seasonal backscatter differences are seen in both overlays. As in Figure 2.5, it can be expected that forested areas in magenta (higher backscatter in summer) consisted mainly of coniferous species and forested areas in green (higher backscatter in winter) were composed mainly of deciduous species.

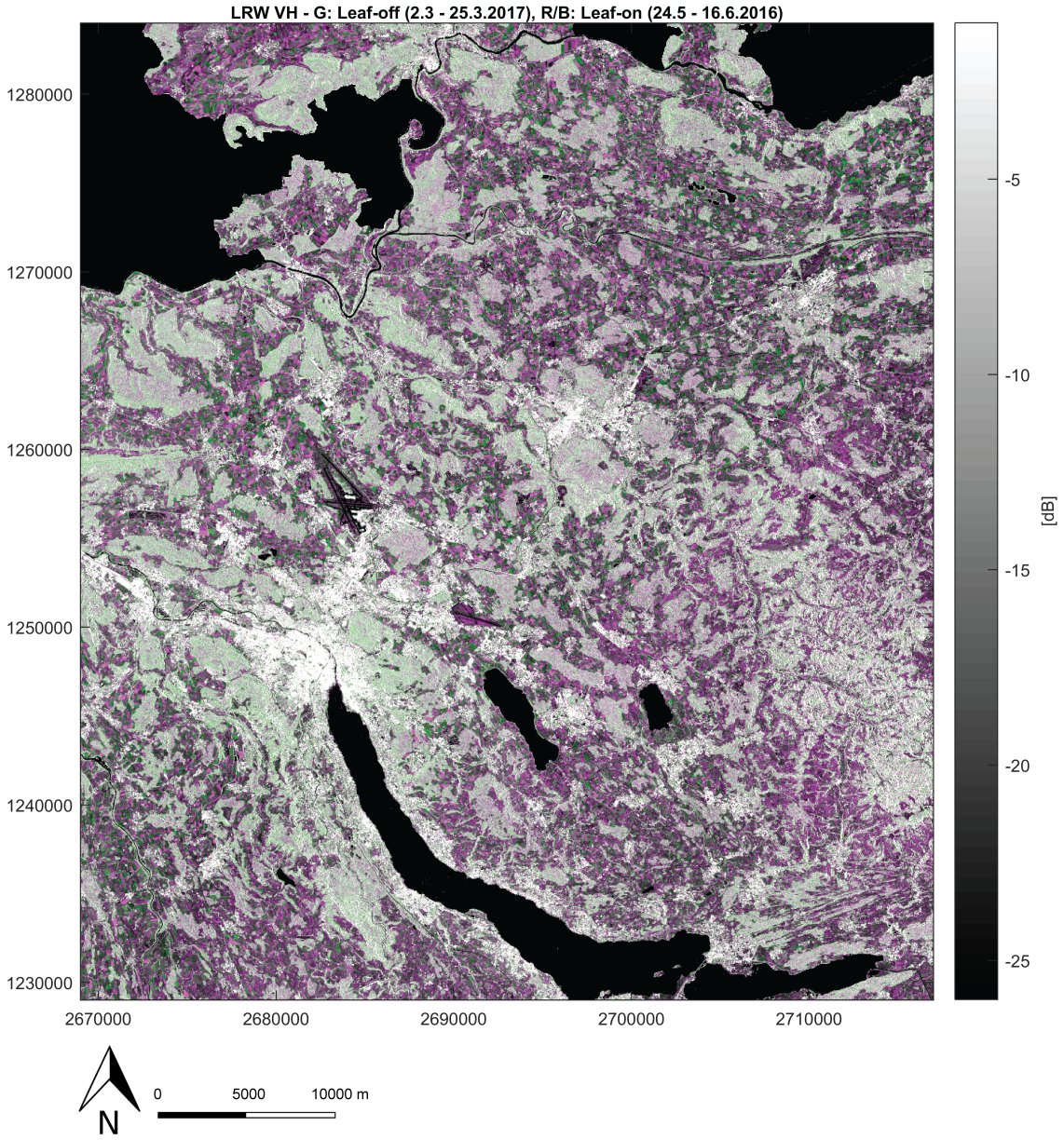

Figure 3.6: Seasonal backscatter differences are seen in the RGB-overlay of two LRW composites of the Canton of Zurich. The assigned bands are R/B = summer/leaf-on (24/05 - 16/06/16) , G = winter/leaf-off (02/03 - 25/03/17). Swiss map coordinates: CH1903+ / LV95.

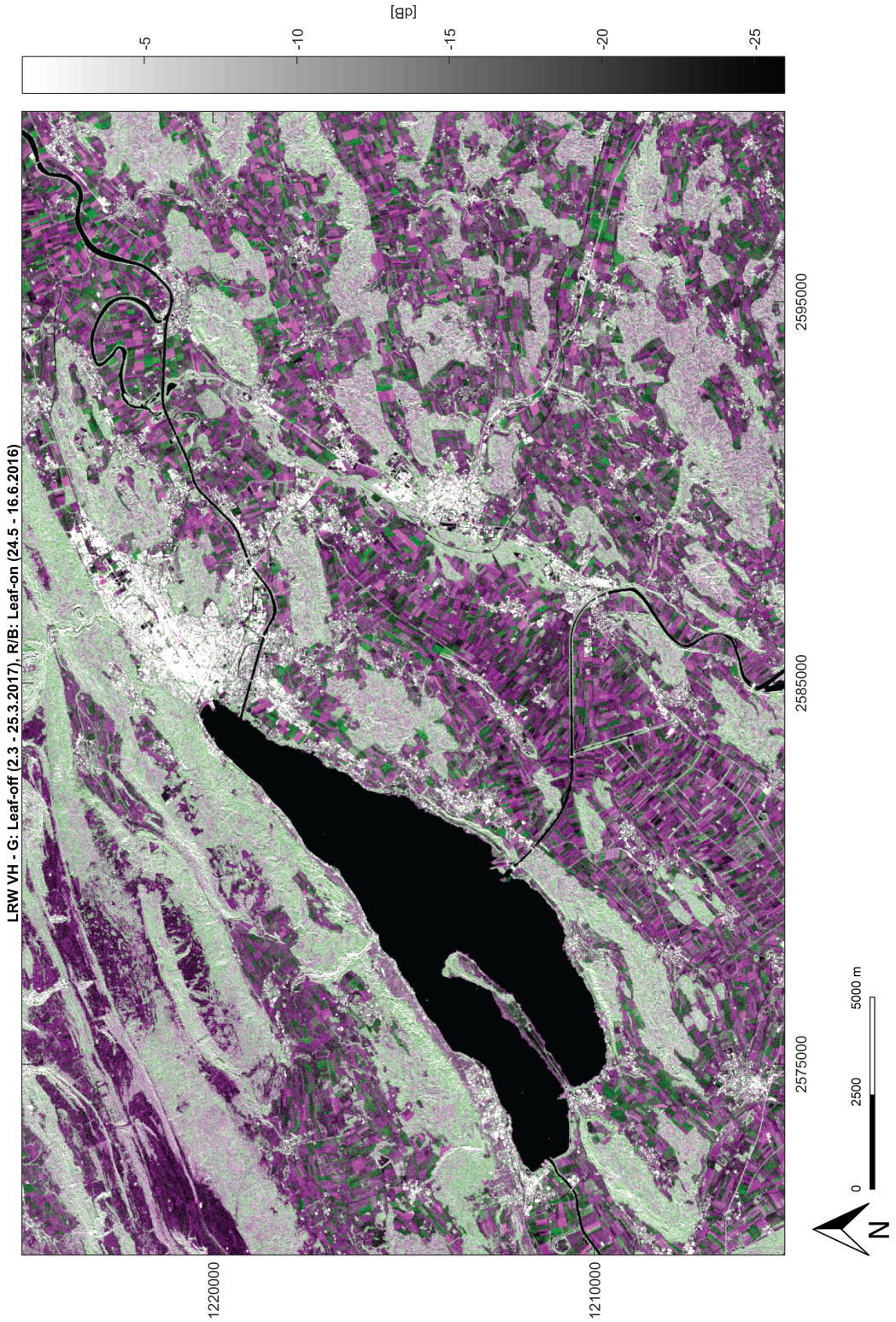

Figure 3.7: Seasonal backscatter differences are seen in the RGB-overlay of two LRW composites of the northwestern part of the Canton of Bern. The assigned bands are R/B = summer/leaf-on (24/05 - 16/06/16) , G = winter/leaf-off (02/03 - 25/03/17). Swiss map coordinates: CH1903+ / LV95.

3.5 Investigations using CORINE land cover classes

3.5.1 Temporal plots of different land cover classes

This section contains additional plots of time series. The temporal backscatter behaviour at both polarisations of level 1 & 2 land cover classes of CORINE land cover (CLC) (Copernicus, 2016) were plotted. The investigated area was the Alpine region (Lat/Lon: 43.5 - 49°N / 5.5 - 17.5°E). The distribution of the different classes within the area is shown in Figure 3.8. The methodology applied was the same as described in section 2.2.3. For the RTC processing, the SRTM DHM was used (Farr et al., 2007), resulting in RTC images with a spatial resolution of 3" (approximately 90 m). The length of the chosen LRW compositing time span was 12 days. Figures 3.9 and 3.10 show the temporal backscatter behaviour from October 2014 to May 2017 of the classes listed in Table 3.4 at VH and VV polarisation, respectively.

Table 3.4: The investigated CLC classes were either of aggregation level 1 or 2. The mean number of available pixels after erosion (see section 2.2.3.2 for details) varied greatly between the classes.

Land cover class	**CLC aggregation level**	**Mean n**
Artificial surfaces	1	2'419'690
Agricultural areas	1	24'512'509
Scrub and/or herbaceous associations	2	5'167'357
Open spaces with little or no vegetation	2	3'488'775
Wetlands	1	137'736
Water bodies	1	9'720'963

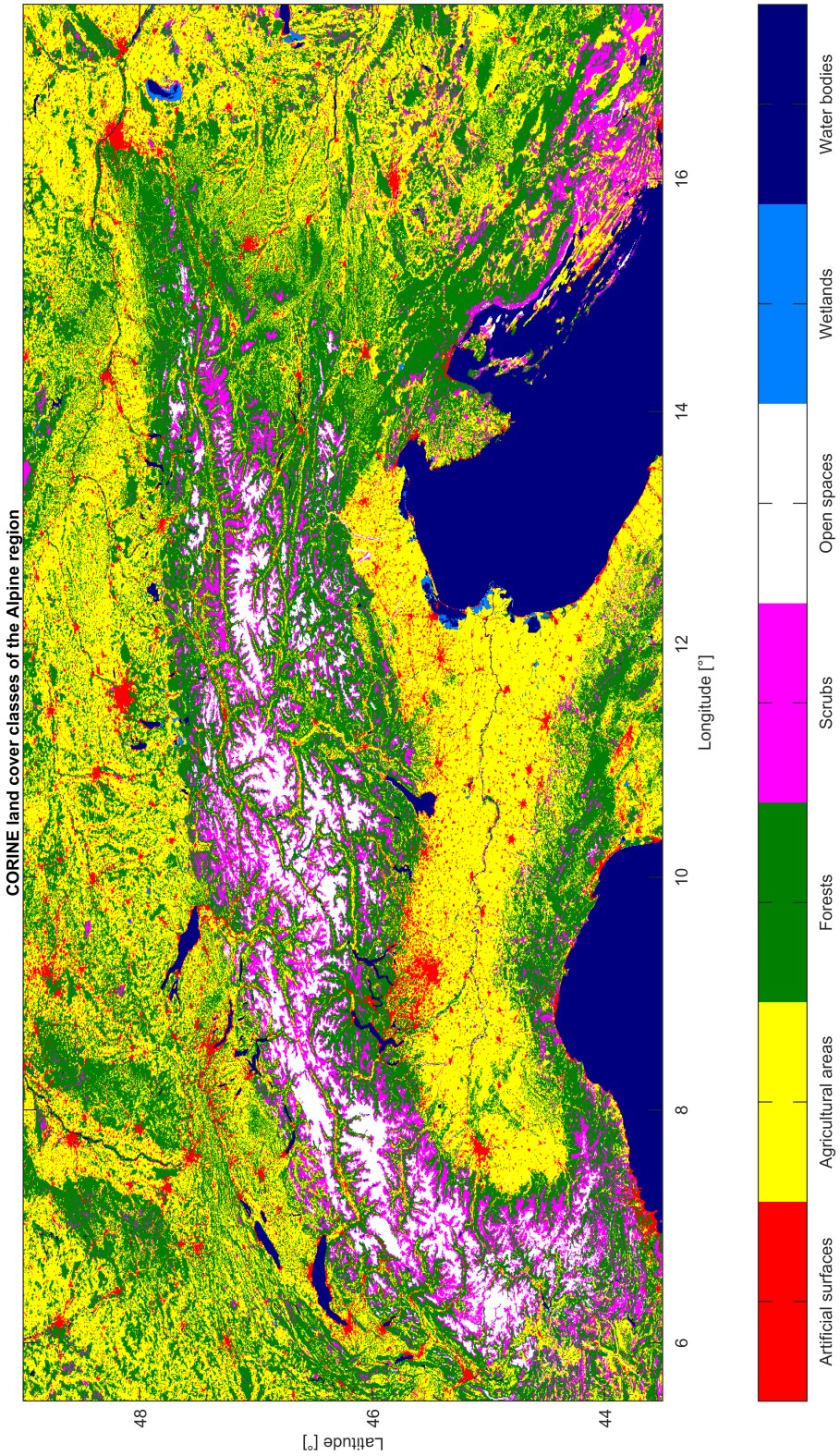

Figure 3.8: Distribution of the CORINE level 1 & 2 land cover classes in the Alpine region before erosion.

The temporal plots in the Figures 3.9 and 3.10 show that backscatter differed between the different land cover classes at VH and VV polarisation. VV backscatter was considerably higher than VH for all land cover types. In addition to the higher values at VV, no considerable difference was observed between the two polarisations for almost all land cover types. Only the backscatter of 'water bodies' differed significantly between the two polarisations.

The land cover classes showed different temporal backscatter behaviours at both polarisations. Temperature effects on the backscatter, such as the lower values in winter 2017, were observed for all land cover types to varying extents. The effect on 'agricultural surfaces' and 'wetlands' were quite strong, while 'artificial surfaces' and 'scrubs' were less affected. No temperature effect was observed on 'open surfaces' and 'water bodies'.

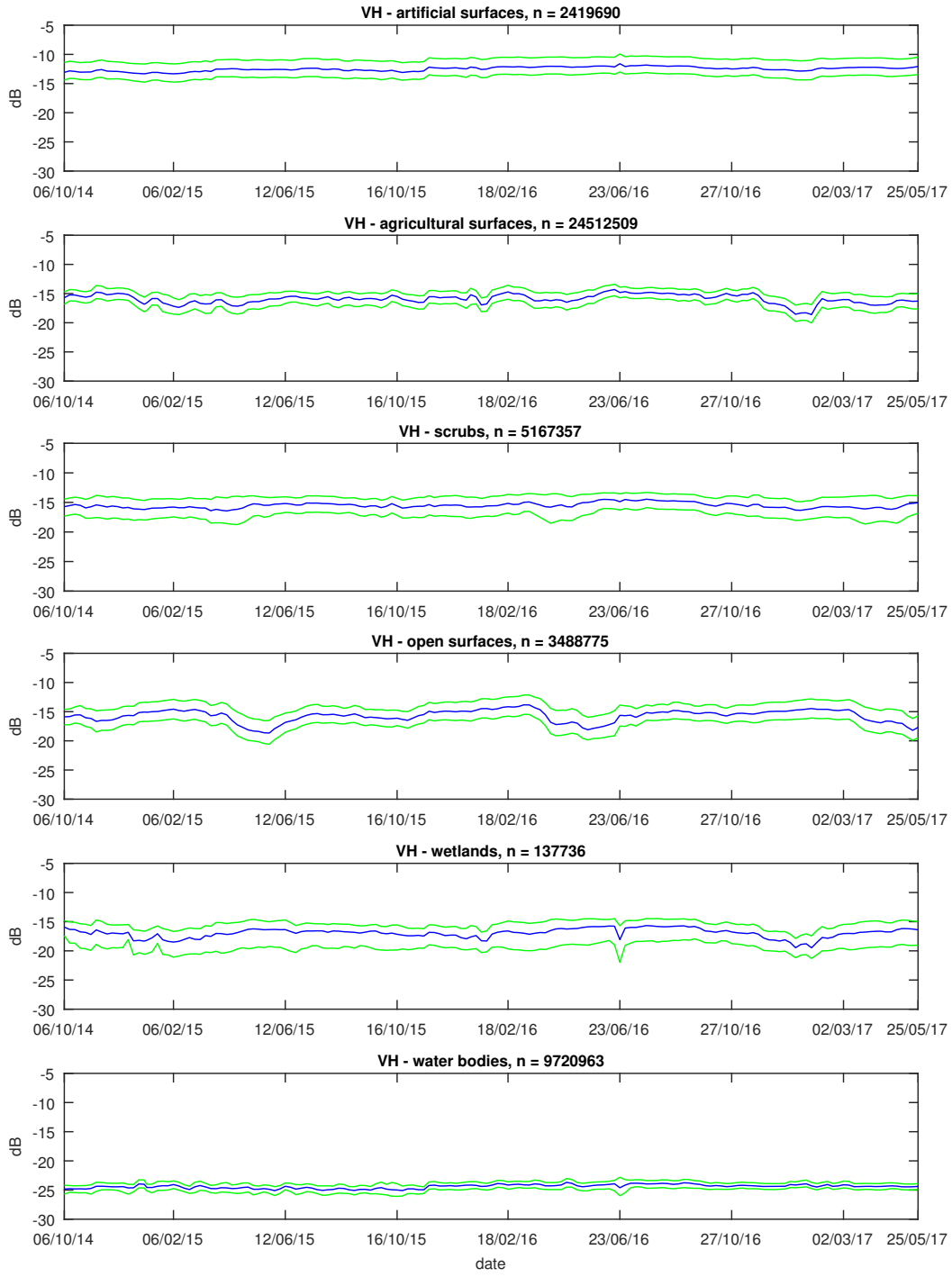

Figure 3.9: Temporal plots of LRW VH composite backscatter for the different land cover classes. Blue shows the median, green corresponds to the 25 & 75% percentiles. The number of investigated pixels (n) varied greatly between the classes.

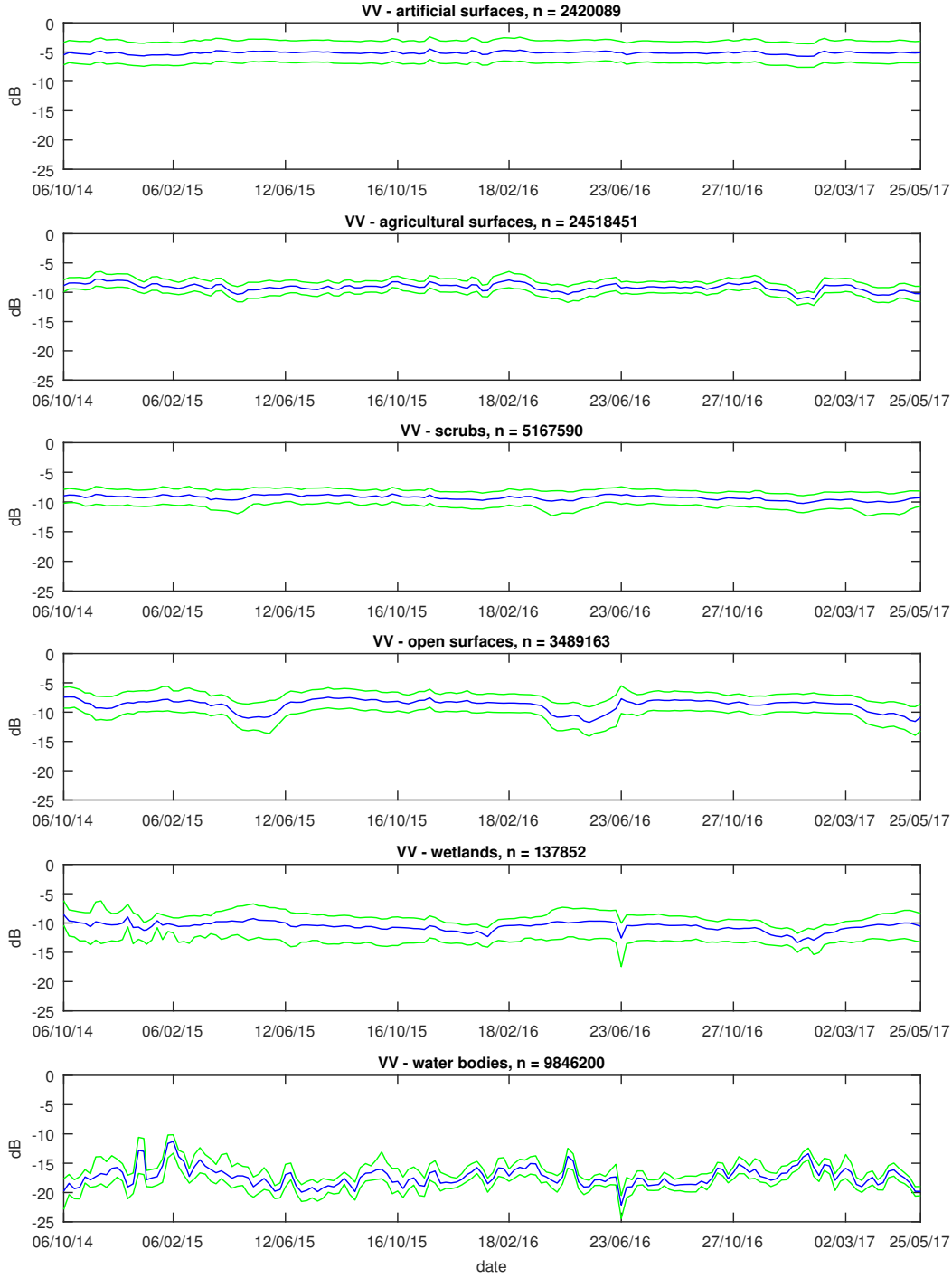

Figure 3.10: Temporal plots of LRW VV composite backscatter for the different land cover classes. Blue shows the median, green corresponds to the 25 & 75% percentiles. The number of investigated pixels (n) varied greatly between the classes.

Backscatter of 'artificial surfaces' was considerably higher than of all the other land cover classes at both polarisations. This is caused by double bounce backscatter in the built-up areas (Clemenz, 2010). In addition to that, the backscatter was stable over time at both polarisations. Contrariwise, large changes in backscatter over time were observed in the class 'agricultural surfaces'. In addition to the mentioned temperature effect, the growth of crops and agricultural practices such as ploughing, sowing and harvesting likely influenced the measured backscatter (Karjalainen et al., 2004). In this case, agricultural surfaces of all crops were aggregated. But investigations of backscatter differences between different crops would be of great interest and would be fruitful in future studies (Liu et al., 2013; Wiseman et al., 2014). C-band backscatter of agricultural surfaces is also influenced by soil moisture content (Balenzano et al., 2011). Thus, differences caused by alterations in soil moisture content should also be further investigated (Navarro et al., 2016; Wang et al., 2016).

A high variance in VH and VV backscatter was observed in 'scrubs' in all three springs. Apart from that, backscatter was rather stable over time with slightly higher values in summer than in winter. 'Open surfaces' also showed stable backscatter over time. In spring, however, periods with significantly lower backscatter values were observed. These lower backscatter values were most probably caused by snowmelt in spring. Koskinen et al. (1997) reported that wet snow leads to a reduction of backscatter of about 3 dB. This effect was observed to such an extent in this class, as most of the areas contained in 'open surfaces' were at high elevations with a lot of snow in winter.

An interesting observation in the plots of 'wetlands' was the difference in width between the median and the 25% percentile, and the median and the 75% percentile. The difference between the latter was smaller than that between the median and the 25% percentile at both polarisations. This might have been caused by low backscatter of extended flooded areas.

Compared to the other classes, 'water bodies' showed lower backscatter values at both polarisations. A large difference between the two polarisations was observed. At VH polarisation, backscatter was stable over time and the variance within each LRW composite was low (narrow band between the 25 & 75% percentiles). At VV polarisation, however, backscatter was unstable and the variance within each composite high. This can be explained by differing influences of Bragg scattering on the polarisations (Curlander & McDonough, 1991).

As already mentioned in section 2.4.7, the same seasonal backscatter patterns in deciduous and coniferous forests were observed over the Alpine region as in the smaller study areas (see section 2.3 for details). Figure 3.11 shows the temporal backscatter behaviour at both polarisations of the two level 3 CLC classes 'broad-leaved forest' and 'coniferous forest'. Broad-leaved, deciduous forests showed a distinct seasonal pattern at VH polarisation with higher backscatter during the leaf-off season and lower during the leaf-on season. At VV polarisation, no distinct seasonal pattern was observed. However, a gradual decrease in backscatter was observed over the leaf-on season. Coniferous forests showed an opposing seasonal backscatter pattern at both polarisations. Backscatter was lower in winter and higher in summer.

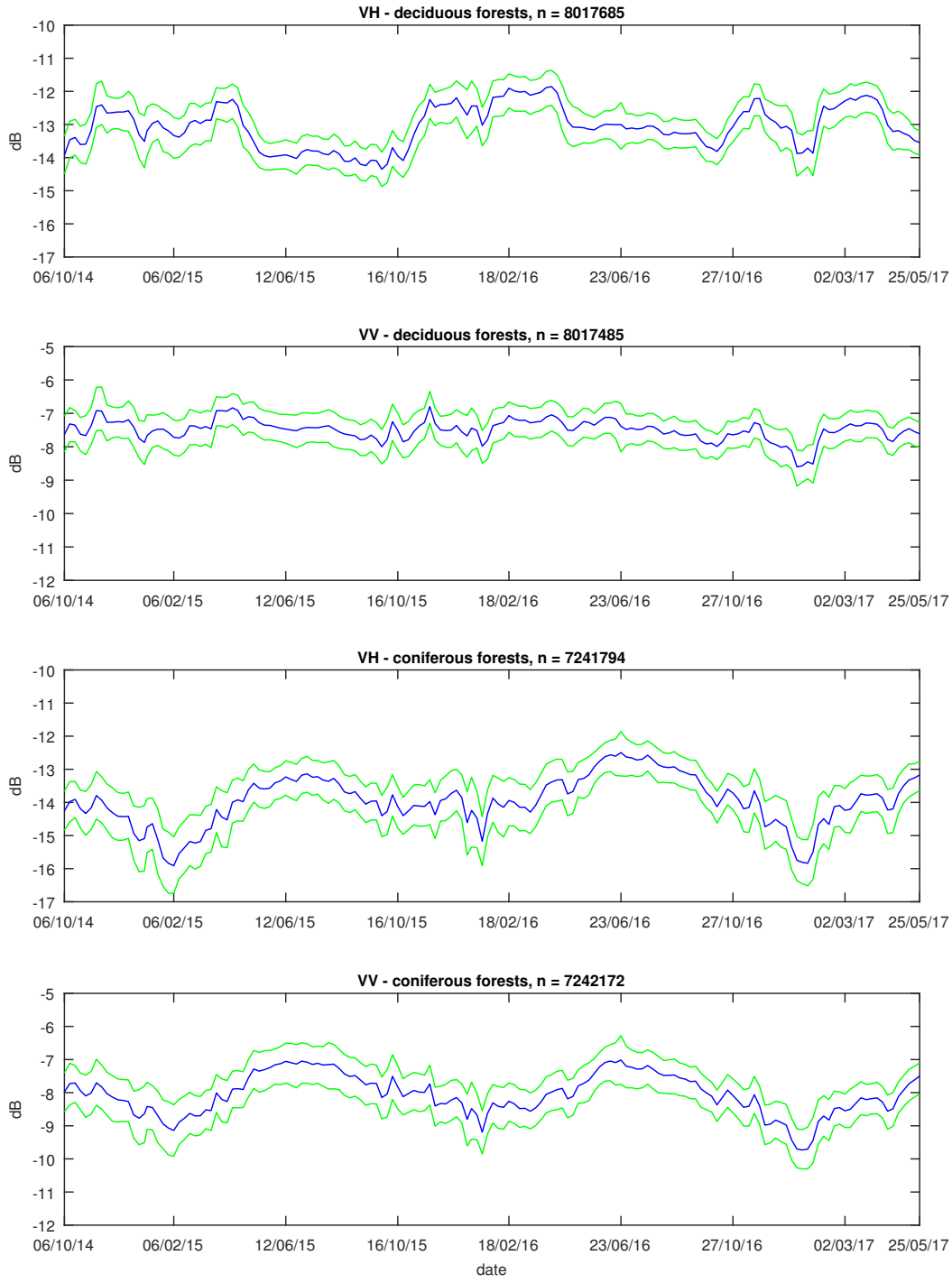

Figure 3.11: Temporal plots of LRW VH and VV composite backscatter for deciduous and coniferous forests. Blue shows the median, green corresponds to the 25 & 75% percentiles. The number of investigated pixels (n) of deciduous forests was higher than of coniferous forests.

3.5.2 Deciduous forests in different elevation ranges

In a further investigation, seasonal VH backscatter patterns of deciduous forests were compared at different elevations. Figure 3.12 depicts the temporal backscatter behaviour of the different elevation ranges. To estimate the timing of leaf emergence and leaf fall, break dates were extracted using the same method as described in section 2.2.3.4. The results revealed different lengths of the leaf-on season for the different elevation ranges. Table 3.5 shows the backscatter derived break dates and the length of the leaf-on season for each elevation range. The higher the elevation, the later the leaf emergence and the earlier the leaf fall. This led to shorter leaf-on seasons for deciduous forests at high elevations.

Table 3.5: Comparison of the break dates (BD) extracted from the VH polarisation time series and their difference (δ BD) for different elevation ranges. Values are displayed in day of the year. The listed uncertainty is due to the compositing timespan of 12 days.

	2015			**2016**		
Elevation range (m a.s.l.)	**BD1**	**BD2**	**δ BD**	**BD1**	**BD2**	**δ BD**
0-499	115±6	307±6	192±12	103±6	301±6	198±12
500-999	127±6	301±6	174±12	109±6	301±6	192±12
100-1499	127±6	295±6	168±12	127±6	295±6	168±12
1500-1999	133±6	283±6	150±12	151±6	289±6	138±12

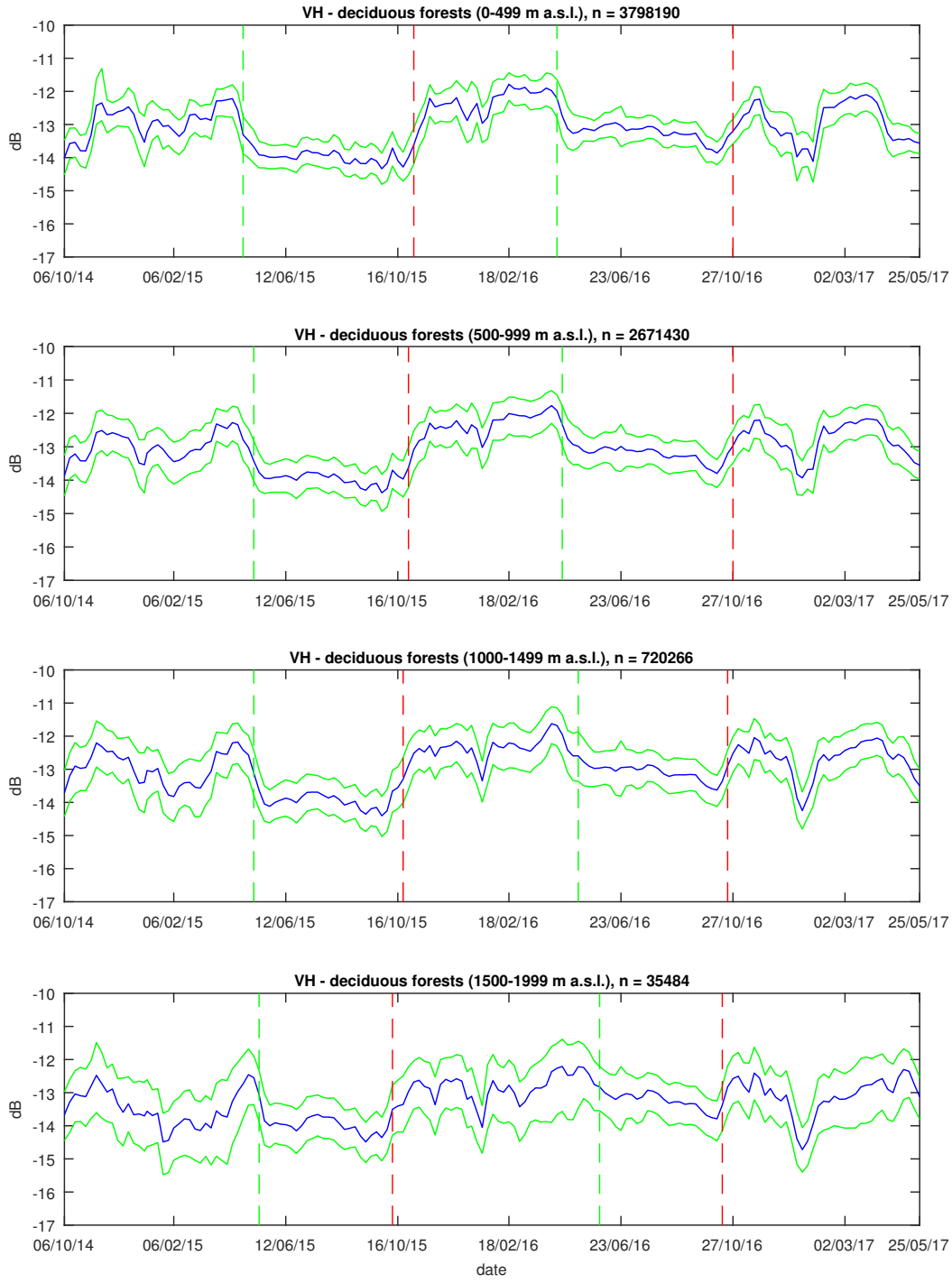

Figure 3.12: Temporal plots of LRW VH composite backscatter for deciduous forests in different elevation ranges. Blue shows the median, green corresponds to the 25 & 75% percentiles. The dashed vertical lines indicate the derived break dates. The number of investigated pixels (n) was considerably lower for deciduous forests in the higher elevation ranges.

3.6 Software used

Most of the calculations for this study were done using MATLAB 2016b (Mathworks, 2016). The rasterisation (see section 2.2.2) and the break date extraction (see section 2.2.3.4) were performed as described below. The rasterisation of the aerial image forest stand map vector layer was conducted using the GDAL algorithm *rasterize* (GDAL, 2017). R (R Core Team, 2017) and the R-packages *strucchange* (Zeileis et al., 2002) and *zoo* (Zeileis et al., 2017) were used to extract the break dates from the VH backscatter time series.

4 | Synthesis

Much potential lies in using multitemporal C-band SAR data to map and monitor ecosystems. ESA's Sentinel-1 mission provides reliable C-band data at VV and VH polarisation for the compilation of consistent time series. Time series of S-1 data were investigated to gain insights into the temporal backscatter behaviour of ecosystems. It was possible to monitor ecosystems and extract *temporal* signatures.

The focus on mixed temperate forests in northern Switzerland showed that the potential of using the time series is especially promising in forested areas. Analysis of the temporal backscatter behaviour revealed that backscatter of deciduous species was higher than of coniferous at both polarisations. In addition, deciduous and coniferous species showed distinctly opposing seasonal backscatter patterns at VH polarisation. The distinct seasonal backscatter pattern of the deciduous species was used to estimate the timing of leaf emergence and leaf fall by extracting break dates from the VH time series. Hence, a monitoring of phenology of the two investigated years was possible. Using the different backscatter signatures of deciduous and coniferous forests, classifications into forest types and species were also possible. The *forest type* classification yielded better results than the *species* one.

Analyses of S-1 time series on a larger spatial scale showed that the same seasonal backscatter patterns were also observed over the whole of the Alpine region. The demonstrated forest classification and break date extraction should also be possible at larger spatial scales. Additional analyses of S-1 time series showed that C-band data has the potential to be used for further land cover types outside of forests. Distinct temporal backscatter behaviours were observed for the investigated land cover classes. Especially in the field of agriculture, methods to accurately monitor or map cultures are in demand (Steele-Dunne et al., 2017). Future research should focus on the extraction of signatures of different crops and the estimation of soil moisture content to assist agriculture management.

Since the end of the commissioning phase of Sentinel-1B in September 2016, the num-

ber of available S-1 acquisitions has been high enough to build time series with a temporal resolution twice as high as the one used for the forest investigation. A combination of S-1 with RADARSAT Constellation Mission data in the near future would further enhance the potential temporal resolution. This enables in-depth studies of ecological processes, such as the leaf emergence and leaf fall or the development of the crown of deciduous species in spring.

In this study, it was possible to investigate time series of 2.5 years in length. In a few years, longer C-band time series will be available. This will facilitate detection of temporal changes in ecosystems with large spatial extents. Consequently, long-term trends caused by climate change, such as shifts of phenophases or changes in species composition in forests, could be observed and quantified using the methodologies shown.

References

Abdikan, S., Sanli, F. B., Ustuner, M., & Calò, F. (2016). Land Cover Mapping Using Sentinel-1 SAR Data. In *International Archives of the Photogrammetry, Remote Sensing and Spatial Information Sciences (ISPRS)*. Prague, Czech Republic: ISPRS, 757–761. DOI: 10.5194/isprsarchives-XLI-B7-757-2016.

Aghabalaei, A., Maghsoudi, Y., & Ebadi, H. (2016). Forest classification using extracted PolSAR features from Compact Polarimetry data. *Advances in Space Research*, *57*(9), 1939–1950. DOI: 10.1016/j.asr.2016.02.007.

Ahern, F., Leckie, D., & Drieman, J. (1993). Seasonal changes in relative C-band backscatter of northern forest cover types. *IEEE Transactions on Geoscience and Remote Sensing*, *31*(3), 668–680. DOI: 10.1109/36.225533.

Antropov, O., Rauste, Y., Astola, H., Praks, J., Hame, T., & Hallikainen, M. T. (2014). Land cover and soil type mapping from spaceborne polsar data at L-band with probabilistic neural network. *IEEE Transactions on Geoscience and Remote Sensing*, *52*(9), 5256–5270. DOI: 10.1109/TGRS.2013.2287712.

Atwood, D. K., Small, D., & Gens, R. (2012). Improving PolSAR land cover classification with radiometric correction of the coherency matrix. *IEEE Journal of Selected Topics in Applied Earth Observations and Remote Sensing*, *5*(3), 848–856. DOI: 10.1109/JSTARS.2012.2186791.

Balenzano, A., Mattia, F., Satalino, G., & Davidson, M. W. J. (2011). Dense temporal series of C- and L-band SAR data for soil moisture retrieval over agricultural crops. *IEEE Journal of Selected Topics in Applied Earth Observations and Remote Sensing*, *4*(2), 439–450. DOI: 10.1109/JSTARS.2010.2052916.

Balzter, H., Cole, B., Thiel, C., & Schmullius, C. (2015). Mapping CORINE land cover from Sentinel-1A SAR and SRTM digital elevation model data using random forests. *Remote Sensing*, *7*(11), 14876–14898. DOI: 10.3390/rs71114876.

Bequet, R., Campioli, M., Kint, V., Vansteenkiste, D., Muys, B., & Ceulemans, R. (2011). Leaf area index development in temperate oak and beech forests is driven by stand characteristics and weather conditions. *Trees - Structure and Function*, *25*(5), 935–946. DOI: 10.1007/s00468-011-0568-4.

Berger, M., Moreno, J., Johannessen, J. A., Levelt, P. F., & Hanssen, R. F. (2012). ESA's sentinel missions in support of Earth system science. *Remote Sensing of Environment*, *120*, 84–90. DOI: 10.1016/j.rse.2011.07.023.

Breiman, L. (2001). Random forests. *Machine Learning*, *45*(1), 5–32. DOI: 10.1023/A:1010933404324.

Bruggisser, M., Roncat, A., Schaepman, M. E., & Morsdorf, F. (2017). Retrieval of higher order statistical moments from full-waveform LiDAR data for tree species classification. *Remote Sensing of Environment*, *196*, 28–41. DOI: 10.1016/j.rse.2017.04.025.

Bush, T., Ulaby, F., Metzler, T., & Stiles, H. (1976). Seasonal Variations of the Microwave Scattering Properties of the Deciduous Trees as Measured in the 1-18 GHz Spectral Range. Tech. rep., Remote Sensing Laboratory, The University of Kansas Space Technology Center, Lawrence, United States.

Cable, J. W., Kovacs, J. M., Shang, J., & Jiao, X. (2014). Multi-temporal polarimetric RADARSAT-2 for land cover monitoring in Northeastern Ontario, Canada. *Remote Sensing*, *6*(3), 2372–2392. DOI: 10.3390/rs6032372.

Chauhan, N. S., Lang, R. H., & Ranson, K. J. (1991). Radar Modeling Of A Boreal Forest. *IEEE Transactions on Geoscience and Remote Sensing*, *29*(4), 627–638. DOI: 10.1109/36.135825.

Chianucci, F., & Cutini, A. (2013). Estimation of canopy properties in deciduous forests with digital hemispherical and cover photography. *Agricultural and Forest Meteorology*, *168*, 130–139. DOI: 10.1016/j.agrformet.2012.09.002.

Chuah, H. T., & Tan, H. S. (1992). A radar backscatter model for forest stands. *Waves in Random Media*, *2*(1), 7–28. DOI: 10.1088/0959-7174/2/1/002.

Clemenz, L. (2010). *Zeitreihenanalyse der Landoberflächensignaturen im Verlauf eines Vegetationszyklus mittels ENVISAT ASAR Daten*. Master's thesis, Remote Sensing Laboratories, Department of Geography, University of Zurich, Switzerland, pp. 139.

Copernicus (2016). CORINE Land Cover 2012.

URL http://land.copernicus.eu/pan-european/corine-land-cover/clc-2012/view, accessed 02/07/2017.

Costanza, R., D'Arge, R., de Groot, R., Farber, S., Grasso, M., Hannon, B., Limburg, K., Naeem, S., O'Neill, R. V., Paruelo, J., Raskin, R. G., Sutton, P., & van den Belt, M. (1997). The value of the world's ecosystem services and natural capital. *Nature*, *387*(6630), 253–260. DOI: 10.1038/387253a0.

Cristiano, P. M., Madanes, N., Campanello, P. I., Di Francescantonio, D., Rodríguez, S. A., Zhang, Y. J., Carrasco, L. O., & Goldstein, G. (2014). High NDVI and potential canopy photosynthesis of South American subtropical forests despite seasonal changes in leaf area index and air temperature. *Forests*, *5*(2), 287–308. DOI: 10.3390/f5020287.

Curlander, J. C., & McDonough, R. N. (1991). *Synthetic Aperture Radar: Systems and Signal processing*. New York, United States: John Wiley & Sons, Inc., pp. 647.

de Jong, R., de Bruin, S., de Wit, A., Schaepman, M. E., & Dent, D. L. (2011). Analysis of monotonic greening and browning trends from global NDVI time-series. *Remote Sensing of Environment*, *115*(2), 692–702. DOI: 10.1016/j.rse.2010.10.011.

de Jong, R., Verbesselt, J., Zeileis, A., & Schaepman, M. E. (2013). Shifts in global vegetation activity trends. *Remote Sensing*, *5*(3), 1117–1133. DOI: 10.3390/rs5031117.

de Lisle, D., & Iris, S. (2016). RADARSAT Constellation Mission Status Update. In *European Conference on Synthetic Aperture Radar (EUSAR)*. Hamburg, Germany: IEEE, 931–933.

Dobson, M., Ulaby, F., LeToan, T., Beaudoin, A., Kasischke, E., & Christensen, N. (1992). Dependence of radar backscatter on coniferous forest biomass. *IEEE Transactions on Geoscience and Remote Sensing*, *30*(2), 412–415. DOI: 10.1109/36.134090.

Dostálová, A., Milenkovic, M., Hollaus, M., & Wagner, W. (2016). Influence of Forest Structure on the Sentinel-1 Backscatter Variation – Analysis With Full-Waveform Lidar Data. In *Living Planet Symposium*. Prague, Czech Republic: ESA.

Drieman, J., Leckie, D., & Ahern, F. (1989). Multitemporal C-SAR for forest typing in eastern Ontario. In *International Geoscience and Remote Sensing Symposium (IGARSS)*. Vancouver, Canada: IEEE, 1376–1378. DOI: 10.1017/CBO9781107415324.004.

El Hajj, M., Baghdadi, N., Zribi, M., & Angelliaume, S. (2016). Analysis of Sentinel-1 Radiometric Stability and Quality for Land Surface Applications. *Remote Sensing*, *8*(5), 1–6. DOI: 10.3390/rs8050406.

Englhart, S., Keuck, V., & Siegert, F. (2011). Aboveground biomass retrieval in tropical forests — The potential of combined X- and L-band SAR data use. *Remote Sensing of Environment*, *115*(5), 1260–1271. DOI: 10.1016/j.rse.2011.01.008.

ESA (2017). Acquisition Modes.
URL https://sentinel.esa.int/web/sentinel/user-guides/sentinel-1-sar/acquisition-modes, accessed 11/05/2017.

Farr, T., Rosen, P., Caro, E., Crippen, R., Duren, R., Hensley, S., Kobrick, M., Paller, M., Rodriguez, E., Roth, L., Seal, D., Shaffer, S., Shimada, J., Umland, J., Werner, M., Oskin, M., Burbank, D., & Alsdorf, D. (2007). The shuttle radar topography mission. *Reviews of Geophysics*, *45*(2), 1–33. DOI: 10.1029/2005RG000183.

Federal Office of Meteorology and Climatology MeteoSwiss (2015). Climate bulletin spring 2015.
URL http://www.meteoschweiz.admin.ch/content/dam/meteoswiss/de/Klima/Gegenwart/Klima-Berichte/doc/klimabulletin_fruehling.pdf, accessed 12/07/2017.

Federal Office of Meteorology and Climatology MeteoSwiss (2016). Climate bulletin spring 2016.
URL http://www.meteoschweiz.admin.ch/content/dam/meteoswiss/de/service-und-publikationen/Publikationen/doc/klimabulletin_fruehling_2016_d.pdf, accessed 12/07/2017.

Federal Office of Meteorology and Climatology MeteoSwiss (2017a). IDAWEB.
URL https://gate.meteoswiss.ch/idaweb/login.do, accessed 01/05/2017.

Federal Office of Meteorology and Climatology MeteoSwiss (2017b). *MeteoSwiss Grid-Data Products: Documentation for Users*. Zurich, Switzerland: MeteoSwiss.

Federal Office of Topography swisstopo (2010). SWISSIMAGE 25.
URL https://www.swisstopo.admin.ch/content/swisstopo-internet/de/home/products/images/ortho/swissimage/_jcr_content/contentPar/tabs/items/dokumente/tabPar/downloadlist/downloadItems/588_1464190449870.download/infosi201003deu.pdf, accessed 12/07/2017.

Federal Office of Topography swisstopo (2017). swissALTI3D.
URL https://www.swisstopo.admin.ch/content/swisstopo-internet/de/home/products/height/alti3d/_jcr_content/contentPar/tabs/items/dokumente/tabPar/downloadlist/downloadItems/846_1464690554132.download/swissALTI3D_detaillierte Produktinfo_2017_de_barrierefrei.pdf, accessed 12/07/2017.

Gamba, P., Dell'Acqua, F., & Trianni, G. (2008). Hypertemporal SAR Sequences for Monitoring Land Cover Dynamics. In *IEEE Radar Conference*. Rome, Italy: IEEE. DOI: 10.1109/RADAR.2008.4720989.

Garonna, I., de Jong, R., & Schaepman, M. E. (2016). Variability and evolution of global land surface phenology over the past three decades (1982-2012). *Global Change Biology*, *22*(4), 1456–1468. DOI: 10.1111/gcb.13168.

GDAL (2017). Geospatial Data Abstraction Library.
URL http://www.gdal.org, accessed 01/05/2017.

Gudex-Cross, D., Pontius, J., & Adams, A. (2017). Enhanced forest cover mapping using spectral unmixing and object-based classification of multi-temporal Landsat imagery. *Remote Sensing of Environment*, *196*, 193–204. DOI: 10.1016/j.rse.2017.05.006.

Hamunyela, E., Verbesselt, J., Roerink, G., & Herold, M. (2013). Trends in spring phenology of western European deciduous forests. *Remote Sensing*, *5*(12), 6159–6179. DOI: 10.3390/rs5126159.

Hansen, A. J., Neilson, R. P., Dale, V. H., Flather, C. H., Iverson, L. R., Currie, D. J., Shafer, S., Cook, R., & Bartlein, P. J. (2001). Global Change in Forests: Responses of Species, Communities, and Biomes. *BioScience*, *51*(9), 765–779. DOI: 10.1641/0006-3568(2001)051[0765:GCIFRO]2.0.CO;2.

Hobi, M. L., Dubinin, M., Graham, C. H., Coops, N. C., Clayton, M. K., Pidgeon, A. M., & Radeloff, V. C. (2017). A comparison of Dynamic Habitat Indices derived from different MODIS products as predictors of avian species richness. *Remote Sensing of Environment*, *195*, 142–152. DOI: 10.1016/j.rse.2017.04.018.

Imhoff, M. L. (1995). A Theoretical Analysis of the Effect of Forest Structure on Synthetic Aperture Radar Backscatter and the Remote Sensing of Biomass. *IEEE Transactions on Geoscience and Remote Sensing*, *33*(2), 341–352. DOI: 10.1109/36.377934.

IPCC (2000). *Land Use, Land-Use Change, and Forestry: A special Report of the IPCC*. [R. T. Watson, I. R. Noble, B. Bolin, N. H. Ravindranath, D. J. Verardo and D. J. Dokken (eds.)], Cambridge University Press, Cambridge, United Kingdom, pp. 375. DOI: 10.2277/0521800838.

IPCC (2014). *Climate Change 2014: Synthesis Report. Contribution of Working Groups I, II and III to the Fifth Assessment Report of the Intergovernmental Panel on Climate Change*. [Core Writing Team, R.K. Pachauri and L.A. Meyer (eds.)], IPCC, Geneva, Switzerland, pp. 151. DOI: 10.1017/CBO9781107415324.

Jäger, D. (2016). *Wide-area wet snow mapping of the Alps based on Sentinel-1 multi-track radar backscatter composites*. Master's thesis, Remote Sensing Laboratories, Department of Geography, University of Zurich, Switzerland, pp. 78.

Karjalainen, M., Kaartinen, H., Hyyppä, J., Laurila, H., & Kuittinen, R. (2004). The Use of Envisat Alternating Polarization SAR Images in Agricultural Monitoring in Comparison With RADARSAT-1 SAR Images. In *International Archives of the Photogrammetry, Remote Sensing and Spatial Information Sciences (ISPRS)*. Istanbul, Turkey: ISPRS, 132–137.

Kasischke, E. S., Melack, J. M., & Dobson, M. C. (1997). The use of imaging radars for ecological applications - A review. *Remote Sensing of Environment*, *59*(2), 141–156. DOI: 10.1016/S0034-4257(96)00148-4.

Kellndorfer, J. M., Pierce, L. E., Dobson, M. C., & Ulaby, F. T. (1998). Toward consistent regional-to-global-scale vegetation characterization using orbital SAR systems. *IEEE Transactions on Geoscience and Remote Sensing*, *36*(5), 1396–1411. DOI: 10.1109/36.718844.

Koskinen, J. T., Pulliainen, J. T., & Hallikainen, M. T. (1997). The Use of ERS-1 SAR Data in Snow Melt Monitoring. *IEEE Transactions on Geoscience and Remote Sensing*, *35*(3), 601–610. DOI: 10.1109/36.581975.

Kovacs, J. M., Jiao, X., Flores-de Santiago, F., Zhang, C., & Flores-Verdugo, F. (2013). Assessing relationships between Radarsat-2 C-band and structural parameters of a degraded mangrove forest. *International Journal of Remote Sensing*, *34*(20), 7002–7019. DOI: 10.1080/01431161.2013.813090.

Kramer, K. (1995). Phenotypic plasticity of the phenology of seven European tree species in relation to climatic warming. *Plant, Cell and Environment*, *18*(2), 93–104. DOI: 10.1111/j.1365-3040.1995.tb00356.x.

Lange, M., Schaber, J., Marx, A., Jäckel, G., Badeck, F. W., Seppelt, R., & Doktor, D. (2016). Simulation of forest tree species' bud burst dates for different climate scenarios: chilling requirements and photo-period may limit bud burst advancement. *International Journal of Biometeorology*, *60*(11), 1711–1726. DOI: 10.1007/s00484-016-1161-8.

Leckie, D., & Ranson, K. (1998). Forestry Applications Using Imaging Radar. In F. Henderson, & A. Lewis (Eds.), *Manual of Remote Sensing: Principles and Applications of Imaging Radar*, New York, United States: John Wiley & Sons, Inc., 435–510. 3rd ed.

Liu, C., Shang, J., Vachon, P. W., & McNairn, H. (2013). Multiyear crop monitoring using polarimetric RADARSAT-2 data. *IEEE Transactions on Geoscience and Remote Sensing*, *51*(4), 2227–2240. DOI: 10.1109/TGRS.2012.2208649.

Lu, D. (2006). The potential and challenge of remote sensing-based biomass estimation. *International Journal of Remote Sensing*, *27*(7), 1297–1328. DOI: 10.1080/01431160500486732.

Luckman, A. J., Baker, J., Kuplich, T. M., Freitas, C., & Frery, A. C. (1997). A Study of the Relationship between

Radar Backscatter and Regenerating Tropical Forest Biomass for Spaceborne SAR Instruments. *Remote Sensing of Environment*, *60*(1), 1–13. DOI: 10.1016/S0034-4257(96)00121-6.

Lüthi, M. (2017). (Local forester, Büren a.d.A., Switzerland). Personal communication.

Maghsoudi, Y., Collins, M. J., & Leckie, D. G. (2013). Radarsat-2 polarimetric SAR data for boreal forest classification using SVM and a wrapper feature selector. *IEEE Journal of Selected Topics in Applied Earth Observations and Remote Sensing*, *6*(3), 1531–1538. DOI: 10.1109/JSTARS.2013.2259219.

Mathworks (2016). *MATLAB 2016b*. Natick, United States: The MathWorks Inc.

Mathworks (2017). TreeBagger documentation.
URL https://ch.mathworks.com/help/stats/treebagger.html, accessed 16/06/2017.

Meier, E., Frei, U., & Nüesch, D. (1993). Precise Terrain Corrected Geocoded Images. In G. Schreier (Ed.), *SAR Geocoding: Data and Systems*, Karlsruhe, Germany: Herbert Wichmann Verlag GmbH, 173–186.

Miranda, N. (2015). S-1A TOPS Radiometric Calibration Refinement#1.
URL https://earth.esa.int/documents/247904/2142675/Sentinel-1A_TOPS_Radiometric_Calibration_Refinement, accessed 12/07/2017.

Moran, M. S., Hymer, D. C., Qi, J., & Sano, E. E. (2000). Soil moisture evaluation using multi-temporal synthetic aperture radar (SAR) in semiarid rangeland. *Agricultural and Forest Meteorology*, *105*(1-3), 69–80. DOI: 10.1016/S0168-1923(00)00189-1.

Mougin, E., Proisy, C., Ducrot, D., Lopes, A., Rivalland, V., Marty, G., Dufrêne, E., Dantec, V. L., Sarti, F., Souyris, J. C., Adragna, F., & Horn, R. (1998). Radar Remote Sensing of a Mixed Deciduous Temperate Forest Results and Perspectives. In *International Workshop on Retrieval of Bio- & Geo-physical Parameters from SAR Data for Land Applications*. Noordwijk, Netherlands: ESA, 285–292.

Muro, J., Canty, M., Conradsen, K., Hüttich, C., Nielsen, A., Skriver, H., Remy, F., Strauch, A., Thonfeld, F., & Menz, G. (2016). Short-Term Change Detection in Wetlands Using Sentinel-1 Time Series. *Remote Sensing*, *8*(10), 1–14. DOI: 10.3390/rs8100795.

Navarro, A., Rolim, J., Miguel, I., Catalao, J., Silva, J., Painho, M., & Vekerdy, Z. (2016). Crop monitoring based on SPOT-5 Take-5 and Sentinel-1A data for the estimation of crop water requirements. *Remote Sensing*, *8*(6), 1–20. DOI: 10.3390/rs8060525.

Office of Landscape, Agriculture and Environment (2010). *Luftbild-Bestandeskarte*. Zurich, Switzerland: Canton of Zurich.

Olesk, A., Voormansik, K., Põhjala, M., & Noorma, M. (2015). Forest change detection from Sentinel-1 and ALOS-2 satellite images. In *Asia-Pacific Conference on Synthetic Aperture Radar (APSAR)*. Singapore, Singapore: IEEE, 522–527. DOI: 10.1109/APSAR.2015.7306263.

Ploberger, W., & Krämer, W. (1992). The CUSUM Test with OLS Residuals. *Econometrica*, *60*(2), 271–285. DOI: 10.2307/2951597.

Proisy, C., Mougin, E., Dufrêne, E., & Dantec, V. L. (2000). Monitoring seasonal changes of a mixed temperate forest using ERS SAR observations. *IEEE Transactions on Geoscience and Remote Sensing*, *38*(1), 540–552. DOI: 10.1109/36.823949.

R Core Team (2017). R: A Language and Environment for Statistical Computing.
URL https://cran.r-project.org/doc/manuals/fullrefman.pdf, accessed 03/07/2017.

Reiche, J., Member, S., Souza, C. M., Hoekman, D. H., Member, S., Verbesselt, J., Persaud, H., & Herold, M. (2013). Feature Level Fusion of Multi-Temporal ALOS PALSAR and Landsat Data for Mapping and Monitoring of Tropical Deforestation and Forest Degradation. *IEEE Journal of Selected Topics in Applied Earth Observations and Remote Sensing*, *6*(5), 2159–2173. DOI: 10.1109/JSTARS.2013.2245101.

Rignot, E., Williams, C., Way, J., & Viereck, L. (1994). Mapping of forest types in Alaskan boreal forests using SAR imagery. *IEEE Transactions on Geoscience and Remote Sensing*, *32*(5), 1051–1059. DOI: 10.1109/36.312893.

Rondeau-Genesse, G., Trudel, M., & Leconte, R. (2016). Monitoring snow wetness in an Alpine Basin using combined C-band SAR and MODIS data. *Remote Sensing of Environment*, *183*, 304–317. DOI: 10.1016/j.rse.2016.06.003.

Roth, K. L., Roberts, D. A., Dennison, P. E., Peterson, S. H., & Alonzo, M. (2015). The impact of spatial resolution on the classification of plant species and functional types within imaging spectrometer data. *Remote Sensing of Environment*, *171*, 45–57. DOI: 10.1016/j.rse.2015.10.004.

Schneider, J. (2016). (Office of forest of the Canton of Bern, Zollikofen, Switzerland). Personal communication.

Schubert, A., Miranda, N., Geudtner, D., & Small, D. (2017). Sentinel-1A/B Combined Product Geolocation Accuracy. *Remote Sensing*, *9*(6), 1–16. DOI: 10.3390/rs9060607.

Schwerdt, M., Schmidt, K., Tous Ramon, N., Klenk, P., Yague-Martinez, N., Prats-Iraola, P., Zink, M., & Geudtner, D. (2017). Independent System Calibration of Sentinel-1B. *Remote Sensing*, *9*(6), 1–34. DOI:

10.3390/rs9060511.

Sharma, R., Leckie, D., Hill, D., Crooks, B., Bhogal, A. S., Arbour, P., & D'eon, S. (2005). Hyper-Temporal Radarsat SAR data of a Forested Terrain. In *International Workshop on the Analysis of Multi-Temporal Remote Sensing Images*. Biloxi, United States: IEEE, 71–75. DOI: 10.1109/AMTRSI.2005.1469843.

Small, D. (2011). Flattening Gamma: Radiometric terrain correction for SAR imagery. *IEEE Transactions on Geoscience and Remote Sensing*, *49*(8), 3081–3093. DOI: 10.1109/TGRS.2011.2120616.

Small, D. (2012). SAR backscatter multitemporal compositing via local resolution weighting. In *International Geoscience and Remote Sensing Symposium (IGARSS)*. Munich, Germany: IEEE, 4521–4524. DOI: 10.1109/IGARSS.2012.6350465.

Solimini, D. (2016). *Understanding Earth Observation*. Basel, Switzerland: Springer International Publishing, pp. 703. DOI: 10.1007/978-3-319-25633-7.

Steele-Dunne, S. C., McNairn, H., Monsivais-Huertero, A., Judge, J., Liu, P. W., & Papathanassiou, K. (2017). Radar Remote Sensing of Agricultural Canopies: A Review. *IEEE Journal of Selected Topics in Applied Earth Observations and Remote Sensing*, *10*(5), 2249–2273. DOI: 10.1109/JSTARS.2016.2639043.

Stenger, A., Harou, P., & Navrud, S. (2009). Valuing environmental goods and services derived from the forests. *Journal of Forest Economics*, *15*(1-2), 1–14. DOI: 10.1016/j.jfe.2008.03.001.

Thiel, C., & Schmullius, C. (2016). The potential of ALOS PALSAR backscatter and InSAR coherence for forest growing stock volume estimation in Central Siberia. *Remote Sensing of Environment*, *173*, 258–273. DOI: 10.1016/j.rse.2015.10.030.

Thom, D., Rammer, W., Dirnböck, T., Müller, J., Kobler, J., Katzensteiner, K., Helm, N., & Seidl, R. (2016). The impacts of climate change and disturbance on spatio-temporal trajectories of biodiversity in a temperate forest landscape. *Journal of Applied Ecology*, *54*(1), 28–38. DOI: 10.1111/1365-2664.12644.

Torbick, N., Chowdhury, D., Salas, W., & Qi, J. (2017). Monitoring Rice Agriculture across Myanmar Using Time Series Sentinel-1 Assisted by Landsat-8 and PALSAR-2. *Remote Sensing*, *9*(2), 1–22. DOI: 10.3390/rs9020119.

Torres, R., Snoeij, P., Geudtner, D., Bibby, D., Davidson, M., Attema, E., Potin, P., Rommen, B. Ö., Floury, N., Brown, M., Traver, I. N., Deghaye, P., Duesmann, B., Rosich, B., Miranda, N., Bruno, C., L'Abbate, M., Croci, R., Pietropaolo, A., Huchler, M., & Rostan, F. (2012). GMES Sentinel-1 mission. *Remote Sensing of Environment*, *120*, 9–24. DOI: 10.1016/j.rse.2011.05.028.

Touzi, R., Landry, R., & Charbonneau, F. J. (2004). Forest type discrimination using calibrated C-band polarimetric SAR data. *Canadian Journal of Remote Sensing*, *30*(3), 543–551. DOI: 10.5589/m03-072.

Vanoni, M., Bugmann, H., Nötzli, M., & Bigler, C. (2016). Quantifying the effects of drought on abrupt growth decreases of major tree species in Switzerland. *Ecology and Evolution*, *6*(11), 3555–3570. DOI: 10.1002/ece3.2146.

Varghese, A. O., & Joshi, A. K. (2015). Polarimetric classification of C-band SAR data for forest density characterization. *Current Science*, *108*(1), 100–106.

Verhegghen, A., Eva, H., Ceccherini, G., Achard, F., Gond, V., Gourlet-Fleury, S., & Cerutti, P. O. (2016). The Potential of Sentinel Satellites for Burnt Area Mapping and Monitoring in the Congo Basin Forests. *Remote Sensing*, *8*(12), 1–22. DOI: 10.3390/rs8120986.

Wang, H., Allain-Bailhache, S., Méric, S., & Pottier, E. (2016). Soil Parameter Retrievals Over Bare Agricultural Fields Using Multiangular RADARSAT-2 Dataset. *IEEE Journal of Selected Topics in Applied Earth Observations and Remote Sensing*, *9*(12), 5666–5676. DOI: 10.1109/JSTARS.2016.2525000.

Waske, B., & Braun, M. (2009). Classifier ensembles for land cover mapping using multitemporal SAR imagery. *ISPRS Journal of Photogrammetry and Remote Sensing*, *64*(5), 450–457. DOI: 10.1016/j.isprsjprs.2009.01.003.

Way, J., Parist, J., Kasischke, E., Slaughter, C., Viereck, L., Christensen, N., Dobson, M. C., Ulaby, F., Richards, J., Milne, A., Sieber, A., Ahern, F. J., Simonett, D., Hoffer, R., Imhoff, M., & Weber, J. (1990). The effect of changing environmental conditions on microwave signatures of forest ecosystems: preliminary results of the March 1988 Alaskan aircraft SAR experiment. *International Journal of Remote Sensing*, *11*(7), 1119–1144. DOI: 10.1080/01431169008955084.

Wegmüller, U., Holecz, F., Wan, Y., & Kattenborn, G. (1994). Theoretical sensitivity of ERS-1 SAR backscatter over forest. In *International Geoscience and Remote Sensing Symposium (IGARSS)*. Pasadena, United States: IEEE, 2477–2479. DOI: 10.1109/IGARSS.1994.399774.

Weiss, M., & Baret, F. (2017). CAN_EYE V6.4.7 User manual.
URL http://www6.paca.inra.fr/can-eye/Media/fichiers/CAN_EYE_User_Manual_V6.4, accessed 03/07/2017.

Westman, W. E., & Paris, J. F. (1987). Detecting forest structure and biomass with C-band multipolarization Radar: Physical model and field tests. *Remote Sensing of Environment*, *22*(2), 249–269. DOI: 10.1016/0034-4257(87)90061-7.

White, M. A., de Beurs, K. M., Didan, K., Inouye, D. W., Richardson, A. D., Jensen, O. P., O'Keefe, J., Zhang, G., Nemani, R. R., van Leeuwen, W. J. D., Brown, J. F., de Wit, A., Schaepman, M., Lin, X., Dettinger, M., Bailey, A. S., Kimball, J., Schwartz, M. D., Baldocchi, D. D., Lee, J. T., & Lauenroth, W. K. (2009). Intercomparison, interpretation, and assessment of spring phenology in North America estimated from remote sensing for 1982-2006. *Global Change Biology*, *15*(10), 2335–2359. DOI: 10.1111/j.1365-2486.2009.01910.x.

Wiseman, G., McNairn, H., Homayouni, S., & Shang, J. (2014). RADARSAT-2 Polarimetric SAR response to crop biomass for agricultural production monitoring. *IEEE Journal of Selected Topics in Applied Earth Observations and Remote Sensing*, *7*(11), 4461–4471. DOI: 10.1109/JSTARS.2014.2322311.

Zeileis, A., Grothendieck, G., Ryan, J. A., Ulrich, J. M., & Andrews, F. (2017). zoo: S3 Infrastructure for Regular and Irregular Time Series (Z's Ordered Observations).
URL https://cran.r-project.org/web/packages/zoo/index.html, accessed 03/07/2017.

Zeileis, A., Kleiber, C., Krämer, W., & Hornik, K. (2003). Testing and dating of structural changes in practice. *Computational Statistics and Data Analysis*, *44*(1-2), 109–123. DOI: 10.1016/S0167-9473(03)00030-6.

Zeileis, A., Leisch, F., Hornik, K., & Kleiber, C. (2002). strucchange: An R Package for Testing for Structural Change in Linear Regression Models. *Journal of Statistical Software*, *7*, 1–38. DOI: 10.18637/jss.v007.i02.

Zwahlen, M. (2017). (Local forester, Ins, Switzerland). Personal communication.

Acknowledgements

The evolution of this thesis was only possible with the generous help of several people. First and foremost, I would like to thank my supervisor David Small for his valuable support throughout the whole working and learning process. He was always available to competently answer my numerous questions. I also want to thank Michael Schaepman for his valuable inputs towards the end that helped the thesis to take form.

Further, I want to express my gratitude to several people from the RSL. I would like to thank Rogier de Jong for providing me with data and advice concerning time series analysis; Reik Leiterer for his help using CAN_EYE to process the hemispherical images; and Christoph Rohner for supplying me with MATLAB scripts and spending time to help me solve my LaTeX issues. I also want to thank Sanne Diek for her R script to generate an inset map; Fabian Schneider for making his LaTeX template available to me and answering questions regarding the acquisitions of hemispherical images; and Benjamin Kellenberger for helping me getting my classification right. Likewise I thank Daniel Kükenbrink for his useful inputs; Giulia Ghielmetti for patiently handing the field work equipment over to me again and again; and Bruno Weber for his reliable IT support.

Moreover, I would like to thank Christof Bigler from the forest ecology group of the ETH for illustrating the process of leaf emergence and providing information about available phenological data. Sincere thanks also go to Denise Lüthy and Jürg Schneider, for providing me with information about the forests in the Canton of Zurich and Bern, respectively.

Further, I want to thank all my friends at University for the nice and challenging time we spent together in the last six years. Special thanks go to Moritz Bruggisser for pointing out ambiguities in my manuscript and helping me with my LaTeX problems; Andrea Millhäusler for detailed proofreading; and Basil Kraft for swapping ideas concerning the thesis.

Last but not least, I would like to thank my parents for allowing me the opportunity to study, which must not be taken for granted, and my whole family for their continuous support during my studies. In this context, Angela deserves special thanks for calming me down and assuring me I was on the right path in times of stress and uncertainty.

Personal Declaration

I hereby declare that the submitted thesis is the result of my own, independent work. All external sources are explicitly acknowledged in the thesis.

Place, Date Signature